

THE FLORIDA STATE UNIVERSITY
COLLEGE OF ARTS AND SCIENCES

OBSERVATION OF MESOSCALE OCEAN DYNAMICS IN THE
NORTHEAST PACIFIC USING GEOSAT RADAR ALTIMETRY DATA

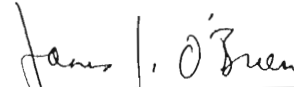
By

PAUL E. MATTHEWS

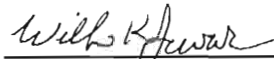
A Thesis submitted to the
Department of Oceanography
in partial fulfillment of the requirements
for the degree of Master of Science

Degree Awarded:
Fall Semester, 1991

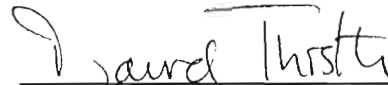
The members of the Committee approve the thesis of Paul E. Matthews , defended on September 6, 1991.



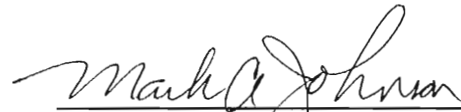
James J. O'Brien
Professor Directing Thesis



William K. Dewar
Committee Member



David Thistle
Committee Member



Mark A. Johnson
Committee Member

Approved:



William C. Burnett, Chair, Department of Oceanography

William C. Burnett, Chair, Department of Oceanography

To my wife Carol

Acknowledgement

This work was supported by The Office of Naval Research, NASA Oceanic Processes, and the National Science Foundation under grant OCE-8811316. Computer time was supplied by The Florida State University's Cray Y-MP.

I wish to express my deepest gratitude to Dr. James J. O'Brien, my major professor and thesis advisor. His advice, motivation and support throughout my two years at Florida State University are greatly appreciated. I also wish to thank Dr. William K. Dewar, Dr. David Thistle and Dr. Mark A. Johnson for taking the time to serve on my committee.

I want to thank my wife and other members of my family for their support and prayers during my two years at Florida State.

I want to thank Dr. Heyward Mathews for giving me the inspiration to pursue a career in Oceanography more than 20 years ago. I would also like to thank Dr. Mathews and Dr. Dan Sheehy for their advice and counsel while I have been a graduate student. I want to thank my colleagues at the Mesoscale Air-Sea interaction Group for their friendship and constructive comments and suggestions. In particular I would like to thank Dr. Mark Johnson, his advice and guidance have been most helpful in the completion of this work. My appreciation is also extended to Dr. Laury Miller and Mr. Bob Cheney and others at NOAA/NOS for providing the data for this research and also for the guidance they gave me on several occasions. Additionally I would like to thank Mr. Alan Davis for all of his computer research and also for the guidance they gave me on several occasions. Additionally I would like to thank Mr. Alan Davis for all of his computer and technical assistance.

Table of Contents

	Page
Acknowledgement	iv
List of Figures	vii
Abstract	xi
1. Introduction	1
1.1 Motivation and Objectives	1
1.2 Review of the Circulation of the Northeast Pacific.....	5
1.2.1 The California Current System.....	10
1.2.2 Alaska Current.....	15
2. GEOSAT	18
2.1 Review of GEOSAT Mission	18
2.2 Using GEOSAT to Observe Mesoscale Ocean Dynamics.....	24
3. GEOSAT Data and Analysis Methods	29
3.1 GEOSAT Data	29
3.1.1 Binned GEOSAT Data	29
3.1.2 Collinear GEOSAT Data.....	32
3.2 Data Analysis Techniques	35
3.2.1 Complex Empirical Orthogonal Functions	35
3.2.2 Two-Dimensional Spectral Analysis	37
3.2.1 Complex Empirical Orthogonal Functions	35
3.2.2 Two-Dimensional Spectral Analysis.....	37
4. Results	38

4.1	Visual Analysis of Binned GEOSAT Data.....	38
4.2	CEOF Analysis of Binned GEOSAT Data	40
4.3	Two-Dimensional Spectral Analysis of GEOSAT Data.....	58
4.4	Analysis of Collinear GEOSAT Data in the Gulf of Alaska	62
5.	Comparison of GEOSAT Data to Selected Model Results	70
6.	Conclusions.....	75
7.	References.....	79
8.	Biographical Sketch.....	82

List of Figures

	Page
<p>Fig. 1. Schematic diagram of the surface circulation in the Northeast Pacific relative to 1000db. Notice that the eastward flowing Subarctic Current and the West Wind Drift bifurcate at the coast. This separation of currents in what is called the transition region forms the cyclonic gyre in the Gulf of Alaska and the equatorward flowing California Current. Adapted from <i>Hickey</i>, [1989].</p>	2
<p>Fig. 2. Distribution of the atmospheric pressure at sea-level over the North Pacific. (a) Winter (January) and (b) Summer (July), from <i>Tabata</i> [1976] are based on 22-yr means (1950-1971) of atmospheric pressure. (c) Winter and (d) Spring, mean sea level pressure from <i>Emery and Hamilton</i> [1985], based on 36-years of sea level pressure. The two dots in (c) and (d) mark the locations which were used to calculate the pressure index which is discussed in the text.</p>	7
<p>Fig. 3. The trajectories of eleven of the 23 drifters used by <i>Kirwan et al.</i> [1978]. The trajectories are superimposed on the 0/1000 db mean annual dynamic topography. Note that the drifters deployed in the Subarctic Current stay in the Alaska Current and Gyre. Those that were deployed in the North Pacific Current or southward remained in the subtropical gyre. Also note the one trajectory that traces out a closed eddy, centered at 57°N and 138°W. This is the so called Sitka eddy [<i>Tabata</i>, 1982].</p>	11
<p>Fig. 4. Schematic illustration of the seasonal variation of the boundary currents along the U.S. Pacific coast [<i>Hickey</i>, 1989].</p>	12
<p>Fig. 5. GEOSAT ERM groundtrack for the 2nd repeat cycle. The missing data are due to large off-nadir attitude excursions of the satellite. For different cycles there are different regions for missing data. The groundtrack spacing at the equator is approximately 150 km, from <i>NOAA Technical Memorandum NOS NGS-46</i>, [<i>Cheney et al.</i> 1987].</p>	20
<p>Fig. 6. The frequency response function of the Hanning window used on the binned GEOSAT data. There were 92 passes made in time producing a half-power point corresponding to a period of 55-</p>	20

days. This value was chosen to retain Rossby wave dynamics and mesoscale features which persist two months or longer..... 33

Fig. 7. Composite of GEOSAT SSH data at 45°N, 125°W to 137°W. Two years are shown to emphasize the annual signal. Notice that the maximum variability is in the eastern part of the data domain. Note also that there is a sloping pattern directed towards the upper left part of the plot. This indicates that as sea level anomalies form near the coast they propagate to the west in time. The SSH contours are in centimeters and negative values are dashed..... 42

Fig. 8. First eigenmode at 45°N accounting for 88% of sea level variance. The time axis is in months with month 1 and 13 corresponding to January. The spatial axis is in degrees longitude. a) & b) Real and imaginary components of the temporal pattern. Notice the strong annual signal and the phase shift between the real and imaginary components. c) & d) Real and imaginary components of the spatial pattern. Again note the phase shift between the two components..... 43

Fig. 9. The amplitude of the spatial pattern of the first eigenmode at 45°N. Notice that the maximum variability is at approximately 127°W and that the variability of sea level is greatly reduced well offshore..... 44

Fig. 10. Reconstructed contour of the first eigenmode at 45°N. This picture is produced by combining the temporal and spatial patterns of the first eigenmode. As shown in the spatial pattern, the maximum variability of sea level occurs around 127°W. The annual signal is quite evident, with sea level near the coast being negative in the winter and positive in the summer. For reference purposes the calculated average phase speed is superimposed on the contour of sea level..... 46

Fig. 11. Same as Figure 7, but for 49°N. Notice that the amplitude of the SSH is smaller at this latitude..... 48

Fig. 12. Same as Figure 8, but for 49°N. Notice that in the temporal pattern there is more shorter scale variability observed than at 45°N. 49

Fig. 13. Same as Figure 9, but for 49°N. The most interesting difference of the amplitude at 49°N, compared to 45°N, is that the maximum variability occurs closer to the coast..... 50

Fig. 14. Same as Figure 10, but for 49°N. The first mode of the SSH at 49°N has a faster average phase speed than that at 45°N. Notice there are regions of both slower and faster propagation of sea level

anomalies. A very significant difference compared to 45°N is the evidence of eastward propagation at the western side of the domain. This particular latitude is in the midst of the bifurcation region and the circulation here is confused, thus accounting for the varying structure of the first eigenmode..... 52

Fig. 15. Same as Figures 7 & 11, but for 57°N..... 53

Fig. 16. Same as Figures 8 & 12, but for 57°N. The amplitude of the sea level signal is very small at this latitude and is evident in both the temporal and spatial patterns..... 54

Fig. 17. Same as Figures 9 and 13, but for 57°N. Notice the amplitude at this latitude shows a second maximum of variability several degrees offshore. This is unlike the amplitude at the more southern latitudes. This feature indicates a second energetic region in addition to the coastal region..... 55

Fig. 18. Same as Figures 10 & 14, but for 57°N. The fact that the average phase speed at this latitude is lower than at 45°N is consistent with Rossby wave theory. Note that in the left hand portion of the plot there is evidence of eastward propagation of sea level anomalies. This appears to be consistent with the known circulation at this latitude as explained in the text..... 57

Fig. 19. The contour of the wavenumber/frequency spectra of the first eigenmode of SSH at 45°N. Only the negative wavenumber, positive frequency quadrant is plotted. The theoretical Rossby linear dispersion relation is superimposed on the contour for reference purposes. A value of $c = 2.5 \text{ m s}^{-1}$ is plotted in a), and a value of $c = 4.7 \text{ m s}^{-1}$ is plotted in b). Because there is very little energy in the positive wavenumber quadrant at this latitude, it is not shown. 59

Fig. 20. Same as Figure 19, but for 57°N. Also the value of c has been changed to a) 4.7 m s^{-1} and b) 5.2 m s^{-1} 61

Fig. 21. The region of study showing the selected ascending tracks used in examining the sea level variability along the Alaska and British Columbia coastlines. The three features "A", "B", and "C", are marked to show the westward propagation of sea level anomalies and are discussed in the text. The track numbers are as described by Gower [1989a & b]. 63

Fig. 22. A time/latitude contour of ascending track 173. This track and all are discussed in the text. The track numbers are as described by Gower [1989a & b]. 63

Fig. 22. A time/latitude contour of ascending track 173. This track is the closest complete ascending track to the coastline. The data points are separated by 5 km in space and 17-days in time. The

contour interval is 5 cm. Notice that there are several eddy like features in addition to those that are marked. A particular area of interest is at the northern part of the track. A considerable amount of variability is evident on the annual time scale in this segment of the track. This is evidence of the seasonal variability of the coastal current in this region..... 64

Fig. 23. Same as Figure 22, but for track 172. 65

Fig. 24. Same as Figure 22 and 23, but for track 171. 66

Fig. 25. The combined spatial and temporal patterns of the first eigenmode of the sea level signal produced by the Gulf of Alaska model. An indication of westward propagation of anomalies is observed in the sloping contours as in the GEOSAT data. The mean phase speed of propagation of the model anomalies is faster than the GEOSAT data. Also there is a second area of high variability well offshore which is not evident in the GEOSAT data. This may be due to the fact that the model only contains a remote forcing component. 72

Abstract

In this study GEOSAT altimetry data from the northeast Pacific is examined. The data are of two types: 1) binned data on 1° -latitude by 2° -longitude blocks and 2) collinear track data. The binned data cover the region from 20°N to 60°N and from the North American coastline westward to 150°W . In time the data span from 15 December 1986 to 1 June 1989. These data are examined using computer animation, which reveals a great deal about the variability of the sea surface signal in this region. Because there is evidence of westward propagation of sea level anomalies from the coast, 3 zonal transects of the data are made: 45°N , 49°N and 57°N . Complex empirical orthogonal function analysis at these latitudes reveals phase speed and amplitude information about the anomalies. The first eigenmode of this analysis at each latitude reveals a very strong annual signal. Two-dimensional spectral analysis at 45°N and 57°N is performed on the first eigenmode of the data. From the information revealed by the spectral analysis, it is concluded that there is westward propagation of sea level anomalies at 45°N . The propagating features are annual in frequency and on the order of 1000 km in length. At 57°N westward propagation is evident (as at 45°N), but there is also an eastward component at this latitude. Collinear track data from three ascending satellite tracks that cross the Gulf of Alaska are examined to observe mesoscale features on the order of 100 km. Many features are observed in these tracks which parallel cross the Gulf of Alaska are examined to observe mesoscale features on the order of 100 km. Many features are observed in these tracks which parallel the Canadian and Alaskan coastline. The most notable being the Sitka

eddy. Westward propagation of a number of these features is observed. The results from the analysis of both types of GEOSAT data are compared with other observational data as well as numerical model data. This comparison study emphasizes the value of altimetry data. In particular it was found that altimetry data is useful in verifying computer models of the ocean and documenting their weaknesses.

1. Introduction

1.1 Motivation and objectives

Over the past several years, many studies have been conducted to gain a better understanding of the circulation of the Northeast Pacific Ocean. A subregion of this area and the principle focus of this paper is the Gulf of Alaska. Figure 1 shows the region of this study. This region encompasses several permanent oceanographic features. These include the California Current system, Alaskan Current, Alaskan Gyre, Subarctic Current, West Wind Drift, and a portion of the North Pacific Gyre. In this paper we analyze GEOSAT (for GEOdetic SATellite) data to increase our knowledge of the Northeast Pacific Ocean circulation.

There are several reasons to study this part of the Pacific Ocean. This region is important because it supports a large and diverse commercial and recreational fishery [Mysak, 1986]. The salmon, halibut, pollack, crab, and other indigent ocean species provide millions of dollars in revenue. Mysak [1986] has shown that fluctuations in the circulation of this region directly affect the annual catches of many of the species of sea life harvested. This region is also important for meteorologic reasons. Many of the winter storms in the western U. S. and Canada are of the maritime polar type. The Gulf of Alaska is the primary region for the
Many of the winter storms in the western U. S. and Canada are of the maritime polar type. The Gulf of Alaska is the primary region for the

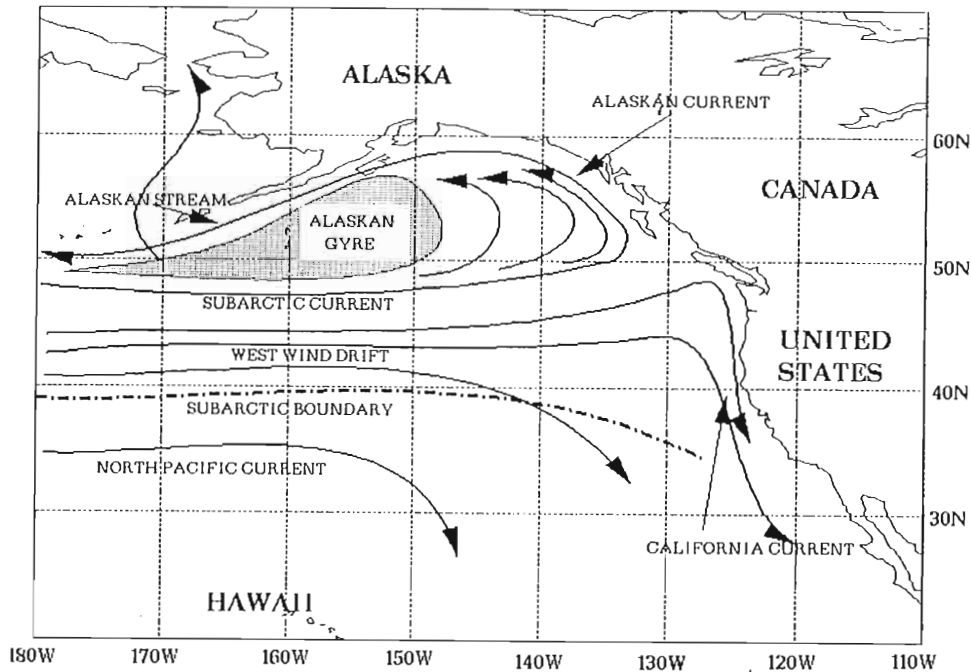


Fig. 1. Schematic diagram of the surface circulation in the Northeast Pacific relative to 1000 db. Notice that the eastward flowing Subarctic Current and the West Wind Drift bifurcate at the coast. This separation of currents in what is called the transition region forms the cyclonic gyre in the Gulf of Alaska and the equatorward flowing California Current. Adapted from *Hickey*, [1989].

genesis of these storms [Aherns, 1982]. In the northern hemisphere winter, cold, dry continental polar air masses form over Asia and the polar regions and are brought southward over the Pacific ocean by the Aleutian Low. As these air masses travel across the ocean, they change their characteristics by acquiring heat and moisture from the ocean. By the time that the air masses reach the Pacific coastline they are cool, moist and unstable. This can result in severe winter storms in the Pacific Northwest, especially in the mountain regions. A better understanding of the ocean's circulation in this region will lead to a better understanding of how the atmosphere responds. This in turn will lead to improved forecasting of these types of winter storms.

Of the circulation studies (of this area) that have been done in the last few years, some have been observational in nature [e.g., Royer, 1981; Tabata, 1982; and Mysak, 1986], while others have been theoretical. The theoretical studies have included both analytic studies and numerical modelling of the region [Cummins and Mysak, 1988]. One of the main drawbacks to both observational and theoretical studies of the circulation of the Gulf of Alaska is that observations of this region have been limited in the past. This is in part due to the region's climate, which can curtail or prevent long-term research cruises. In the past few years, some solutions to this problem of data deficiency have been devised. These include new technologies such as deep moored current meters and satellite tracked buoys [Tabata, 1982], as well as other remote sensing tools.

One of the newest observational tools for determining the ocean's circulation patterns is the satellite borne radar altimeter. The most recent

One of the newest observational tools for determining the ocean's circulation patterns is the satellite borne radar altimeter. The most recent

of these is the satellite called GEOSAT (July, 1991). By measuring the sea surface height (henceforth SSH), which is essentially the shape of the ocean around the earth, as measured by a radar altimeter, an estimate of the geostrophic circulation can be made. Also, mesoscale ocean features can be observed in the SSH. These may include eddies, fluctuations or meanders in mean surface currents, oceanic fronts and planetary waves such as Rossby and Kelvin waves. The purpose of this study is to analyze GEOSAT SSH data taken from the Gulf of Alaska and Northeast Pacific regions and discern specific mesoscale ocean features. Some comparisons of GEOSAT data will be made to other observational data and also to data produced by a numerical model of the same region. The motivation behind these comparisons is to learn how to utilize radar altimeter data in oceanographic research.

This paper is divided into six sections. The remainder of this section presents an overview of the region's circulation. Section two is a review of the GEOSAT mission and some of the recent research using GEOSAT data. Section three presents the two types of GEOSAT data and the analysis techniques used in this research. The first GEOSAT data set is average SSH data binned in 1° -latitude by 2-longitude boxes. This particular data set is analyzed with complex empirical orthogonal functions and two dimensional power spectrum analysis. The second type of data is from several ascending and descending GEOSAT tracks that traverse the area of interest. These data are analyzed using standard time-series techniques. The results of the GEOSAT data analysis will be presented in section four. The results of the GEOSAT data analysis will be presented in section four. We demonstrate evidence of westward propagation of sea level anomalies,

observations of mesoscale eddies and observations of the fluctuations in the mean surface circulation. This section will also include comparison of GEOSAT data to other observational data. We show that the GEOSAT data is in good agreement with classical observations of the area such as those involving drifter data. Section five contains comparisons of GEOSAT results with the sea surface signal produced by numerical models. We show that GEOSAT SSH data is also in good agreement with model solutions of the seasonal variability of the sea level off the Oregon and Washington coastlines. Finally, in section six we present our conclusions.

1.2 Review of the circulation in the Northeast Pacific

The mean atmospheric circulation in the Gulf of Alaska is dominated in the winter by an intense low pressure system known as the Aleutian Low. This system stretches from the Kamchatka Peninsula in Asia all the way to the Pacific coast of North America. To the south of this region is the Subtropical high, which is centered over an area just west of southern California. In the spring, the Aleutian low begins to weaken and shift westward, and the Subtropical high strengthens and expands [Emery and Hamilton, 1985]. By mid-summer, the Subtropical high has intensified due to seasonal warming. The high pressure system now dominates the entire northeast Pacific, and all evidence of the Aleutian low has disappeared from the region. In the fall, the high pressure starts to weaken, and the atmosphere starts to return to the wintertime condition. In the fall, the high pressure starts to weaken, and the atmosphere starts to return to the wintertime condition. Figures 2a - 2d show the seasonal mean sea level atmospheric pressure for

the northeast Pacific.

The most important aspect of this season-to-season atmospheric pattern, as it pertains to this research, is that there is a great deal of variability about the mean atmospheric circulation from one year to the next. *Emery and Hamilton* [1985] examined only the mean winter and mean spring atmospheric pressure from 1947 to 1982 for this region, but their research exemplifies how variable the atmosphere is in this region. They were able to classify three distinct patterns of the sea level atmospheric pressure (SLP) and the related circulation. These are: 1) close to the mean, 2) a greatly intensified Aleutian low, and 3) a weak Aleutian low with an intensified Subtropical high that intrudes into the Gulf of Alaska from the southeast. From the SLP data for the region, a pressure index time series was computed between the two stations marked by dots in Figures 2c and 2d. This pressure index gave a relative strength of the atmospheric circulation and was compared to records of sea surface temperature and sea level at coastal stations in British Columbia (B.C.). The sea level data were taken from Victoria, B.C. and Prince Rupert, B.C. The time series for the pressure index and the sea level at Prince Rupert showed a correlation of 0.68. This correlation was dominated by the fact that when the pressure index was high there was almost always a corresponding high sea level at Prince Rupert. The explanation given for this is that a high pressure index corresponded to strong geostrophic surface wind from the south or southwest. This induced a stronger than normal oceanic mass transport shoreward, which resulted in higher than surface wind from the south or southwest. This induced a stronger than normal oceanic mass transport shoreward, which resulted in higher than normal sea level along the coast. The time series comparison of the data

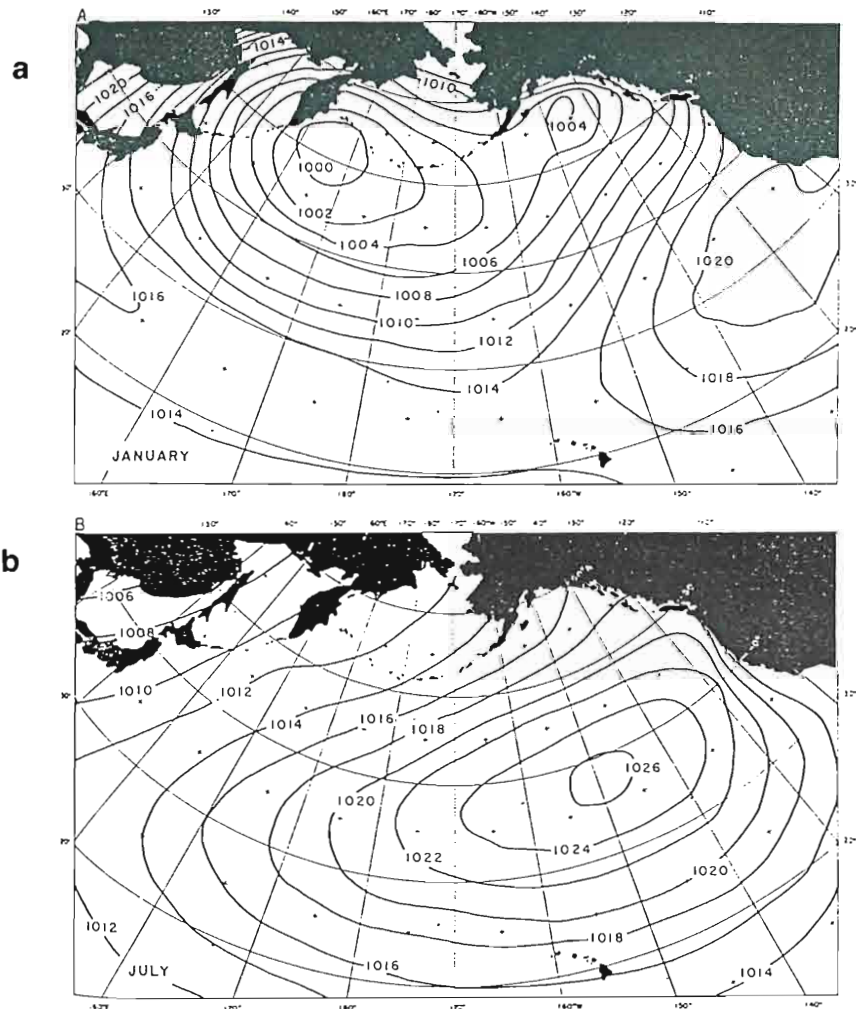


Fig. 2. Distribution of the atmospheric pressure at sea-level over the North Pacific. (a) Winter (January) and (b) Summer (July), from *Tabata*, [1976] are based on 22-yr means (1950-1971) of atmospheric pressure. (c) Winter and (d) Spring, mean sea level pressure from *Emery and Hamilton* [1985], based on 36-years of sea level pressure. The two dots in (c) and (d) mark the locations which were used to calculate the pressure index which is discussed in the text.

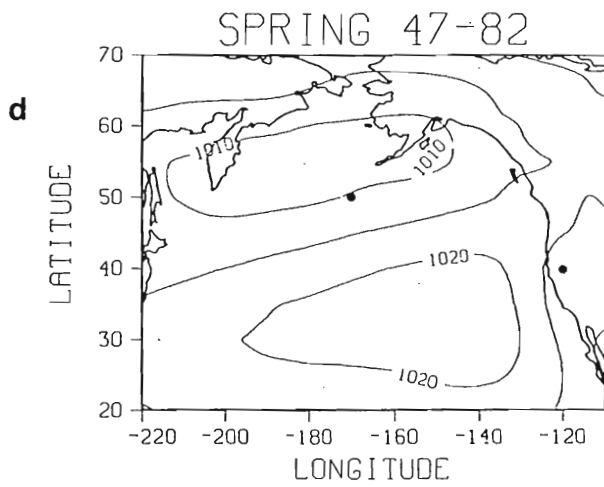
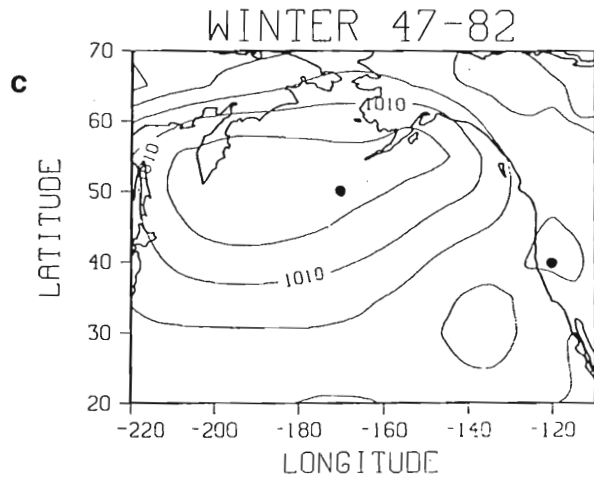


Fig. 2. Continued

also showed that at times the sea level at Prince Rupert was high when the value for the pressure index was low. This led *Emery* and *Hamilton* to believe that there were mechanisms other than the local atmospheric signal that force the sea level in the Northeast Pacific. At Victoria, the correlation between sea level and the pressure index was low (0.28). *Emery* and *Hamilton* concluded that the location of the sea level station (in the Strait of Juan de Fuca) was reflecting many mechanisms, such as local effects, other than atmospheric forcing in the sea surface signal.

If we examine the mean ocean surface circulation of the northeast Pacific, it mirrors (in a geostrophic sense) the atmospheric circulation as described above. Notice that in Figure 1 there is a general cyclonic flow to the north of 45°N and a general anticyclonic flow to the south of that latitude. The mean geostrophic surface winds in the region of 45°N are generally from the south to southwest in both the summer and winter. In the open ocean, the corresponding surface wind stress is ~15°-30° to the left of the geostrophic wind. This induces an oceanic mass transport which is about 90° to the right of the wind stress [*Emery and Hamilton, 1985*]. The resulting mean surface circulation in this region then is the combination of the Subarctic Current, the West Wind drift, and the North Pacific Current. These currents flow eastward and are centered about 45°N. When this flow impinges upon the North American coastline (continental shelf), it bifurcates forming the poleward flowing Alaska Current and the equatorward flowing California Current.

The mean currents described above have been well documented in equatorward flowing California Current.

The mean currents described above have been well documented in the literature. A good example of this is the *Kirwan et al.*, study of 1978.

This study examined the trajectories of 23 satellite tracked drifting buoys that were released in the northeast Pacific ocean. Figure 3 shows the trajectories of eleven such buoys superimposed on the mean annual dynamic topography referenced to 0/1000 db. If we disregard the mesoscale variability of the individual tracks, it is apparent that the drifters followed the mean circulation of the region very well. One point of note about the drifters is that those deployed in the North Pacific current or southward remained in the subtropical gyre, while those that were deployed in the subarctic current or northward remained in the subarctic (or Alaskan) gyre [Kirwan, *et. al.*]. Those that went to the south seemed to follow the path of the California Current, and those that went north followed the Alaska Current and some of these were observed to be entrained in mesoscale eddies. At this point, a more in depth discussion of the California Current and the Alaska Current is warranted.

1.2.1 The California Current system

The California Current in Figure 1 is more accurately described as the California Current system. It is comprised of the California Current (CC), the Davidson Current (DC), and the California Undercurrent (CU), [Hickey, 1989]. In this discussion, the CU will be omitted as this research is focused on the surface circulation in this region. Figure 4 shows the seasonal mean flow of both the CC and the DC. Notice that in winter both of these currents are present. The equatorward flowing CC is furthest from seasonal mean flow of both the CC and the DC. Notice that in winter both of these currents are present. The equatorward flowing CC is furthest from shore and the DC is at its maximum, flowing poleward and skirting the

$$\frac{1}{\rho} \frac{\partial p}{\partial y} = -fu \quad \text{Eq. 2b.}$$

In that this specific research is interested in observing mesoscale ocean features in the Gulf of Alaska, the only measurement from GEOSAT that is used is the variability of the SSH about the mean sea surface. For the region of study, the mean sea surface was taken as the one year mean at each data point for the year August 1987 to August 1988. This definition of the mean was predetermined in the data set which was received from NOAA/NOS. The measurement of SSH is calculated as follows:

$$\eta(x) = H_s - H_g \quad \text{Eq. 3a}$$

where,

$$H_s = H_o(x) - H_a(x) \quad \text{Eq. 3b}$$

and that changes in η (the variability of SSH) are given by,

$$\frac{\partial \eta}{\partial x} = \frac{\partial H_s}{\partial x} - \frac{\partial H_g}{\partial x} \quad \text{Eq. 3c}$$

Calman [1987] defines all of the measurements shown here. H_o is the orbit height of the satellite determined from an ephemeris (a table of satellite positions versus time). H_a is the distance from the satellite to the sea surface measured by the altimeter. H_s is the sea surface relative to the ellipsoid of revolution of the satellite. H_g is the mean geoid height. H_o is the orbit height of the satellite determined from an ephemeris (a table of satellite positions versus time). H_a is the distance from the satellite to the sea surface measured by the altimeter. H_s is the sea surface relative to the ellipsoid of revolution of the satellite. It is the shape that the ocean would have if the ocean were motionless on a rotating earth. H_g is the mean geoid

which is determined from very accurate models or by direct measurements of the earth's gravity field. The dynamic topography, η , is the departure of the sea surface from the mean geoid. Hidden in the measurement of SSH are many complications to receiving sea level information and errors which need to be corrected. Many of these errors are caused by environmental effects, while others are due to instrument design or satellite orbit. The corrections and adjustments that were made to the raw data to produce the Geophysical Data Records (GDR's), which are distributed by NOAA/NOS are explained in full detail in *NOAA Technical Memorandum, NOS, NGS-46*, [Cheney et al., 1987]. The weakest of all corrections made to raw GEOSAT data is the one for the wet troposphere effect.

The error induced by the wet troposphere is one which effects the path-length of a radar pulse sent from the satellite. The moisture in the atmosphere effectively slows the speed of electromagnetic waves travelling from one point to another. This increases the time that it takes for the satellite to receive the reflected energy from the sea surface. The increased time is interpreted by the altimeter as a depression in the sea surface. Therefore, the raw measurement will show an SSH which is lower than it really is. In extreme cases, it is estimated that this error can contribute as much as 35 cm in magnitude to the SSH. This large value can mask some mesoscale features and enhance others. To date there have been four methods utilized to correct the error caused by the wet troposphere.

The first method for correcting the wet tropospheric error was to methods utilized to correct the error caused by the wet troposphere.

The first method for correcting the wet tropospheric error was to utilize data from the U.S. Navy's Fleet Numerical Oceanographic Center

water vapor model. This is a global model which is updated every 12 hours by a large observational data set [Cheney *et al.*, 1987]. The model data for the appropriate time and place, corresponding to altimeter measurements are added to the raw GEOSAT data to make the water vapor correction. The second method employed was based on climatologic water vapor derived from 3 years of NIMBUS-7 SMMR (Scanning Multichannel Microwave Radiometer), observations [Cheney *et al.*, 1987]. The third method for making water vapor corrections has only recently been added to the full set of GDR's and appears to be the most accurate, when available [personal communication with *Laury Miller*]. This method incorporated data taken from the Special Sensor Microwave/Imager (SSM/I), on board the polar-orbiting Defense Meteorological Satellite Program (DMSP), satellite number 8 which began its mission in 1987. Because the DSMP - 8 and GEOSAT missions were concurrent, although not on the same orbit, it was possible to use water vapor data from the SSM/I which corresponded to GEOSAT tracks within a few hours [Phoebus and Hawkins, 1990]. The fourth method to make water vapor corrections is by using the data from the TIROS operational vertical sounder (TOVS) [Emery *et al.* 1990]. The reader is encouraged to see the many articles concerning water vapor corrections which appear in the *GEOSAT Special Issue of the Journal of Geophysical Research*, [1990]. The main point which has been learned from the various research concerning water vapor corrections, is that in areas where the SSH variability is low and the variability of atmospheric water vapor is high, the most accurate corrections available must be made to the raw SSH variability is low and the variability of atmospheric water vapor is high, the most accurate corrections available must be made to the raw GEOSAT data. In the future, radar altimetry satellites should have

onboard radiometers to determine the atmospheric water vapor that is coincident with every radar pulse.

2.2 Using GEOSAT to Observe Mesoscale Ocean Dynamics

One of the first efforts to utilize GEOSAT data in the analysis of ocean features was performed by *Cheney et al.* [1989]. Their main project was to monitor tropical sea level variability, particularly the tropical Pacific Ocean. By 1989 this group had analyzed more than 4 years of data to derive a continuous time series of Tropical Pacific sea level data. By comparing the GEOSAT time series with tide gauge data taken from island stations in the Tropical Pacific a measure of the accuracy of the GEOSAT data was made. After including the necessary error corrections (including the FNOC water vapor for this study), it was found that GEOSAT agreed with the tide gauge data to within 4 - 6 cm rms with a correlation ranging between 0.8 and 0.9. The analysis also showed good agreement when compared to sea level produced by existing wind driven models of the Tropical Pacific.

One of the most enlightening aspects of the *Cheney et al.* [1989], project was the near real time observation of the 1986-87 equatorial El Niño event. For the first time ever, high resolution, direct observations of the evolution of an El Niño event were made. The observation of an equatorial El Niño event by a satellite measuring sea level was predicted by *O'Brien* [1980]. He predicted that, as the southeast trades weaken in the central El Niño event by a satellite measuring sea level was predicted by *O'Brien* [1980]. He predicted that, as the southeast trades weaken in the central Pacific, evidence of the resultant downwelling Kelvin wave would be

observable in the sea level signal measured by a satellite altimeter. By continuously monitoring tropical sea level with a radar altimeter it is predicted that better forecasts of El Niño events will be possible. This is especially true when altimetry data is assimilated into ocean circulation models and compared to other oceanographic observations. As GEOSAT is no longer in service, and there are currently no other satellites with radar altimeters aboard, the monitoring of global sea level in this manner is temporarily on hold (July 1991).

The *Cheney et al.* [1989] project just discussed showed the value of using satellite altimetry data for observing the variability of the SSH on an interannual time scale. There have been numerous studies that examine the variability of the SSH on seasonal and annual time scales e.g., *Zlotnicki et al.* [1989] examined the seasonal variability of sea level for the entire globe using GEOSAT data for the period November 1986 to March 1988. This study is significant because their research showed that the seasonal variability of SSH observed in the NE Pacific was not due to errors in the measuring system. In fact they found, as expected from theory, that the variability of SSH is in phase with the wind stress curl of the region. They also found that the SSH from GEOSAT was consistent with other observational studies, (i.e. current meter studies), and that it provides evidence of the response of the ocean to seasonally fluctuating winds.

Two system errors that *Zlotnicki et al.* [1989] address specifically in their paper are those due to the inverse barometer effect and the water vapor (or wet troposphere) effect. They conclude that if the proper orbit their paper are those due to the inverse barometer effect and the water vapor (or wet troposphere) effect. They conclude that if the proper orbit correction is included in the raw data manipulation then the inverse

barometer effect is negligible. This is because the length scale of atmospheric pressure systems is on the order of 1000 km, and the proper orbit correction tends to eliminate signals of that scale. They also conclude that for this particular region (NE Pacific), the water vapor error does not drastically alter the oceanographic signal. The reasoning behind this is that in regions north of 35° N the water vapor variability, in both time and space, is much lower than in regions to the south of 35° N. This means that the water vapor correction is small for the NE Pacific region compared to elsewhere. This argument is contradicted by *Pheobus and Hawkins*, [1990] with their research using SSM/I data. They found that 42% of the oceanographic features that they observed using GEOSAT data from the NE Pacific during the month of September 1987 were altered in some way by water vapor effects. One explanation for the discrepancy between these two studies is that one examined the seasonal variability while the other was looking at a single month of data. To reiterate a point made earlier, the best available corrections to the water vapor error must be made to GEOSAT data in order to get the best rendering possible of SSH.

Another study examining the seasonal variability of SSH is that of *White et al.* [1990]. They examine evidence of annual Rossby waves in the GEOSAT ERM data in the California Current. Using CEOF analysis, they find that for their 1-year data set (November 1986 to October 1987), that the annual signal accounts for 53% of the variance of SSH, while the semi-annual signal accounts for 23%. They also found, using two dimensional spectrum analysis, that the maximum energy of the sea level signal was annual signal accounts for 23%. They also found, using two dimensional spectrum analysis, that the maximum energy of the sea level signal was qualitatively close to the linear Rossby dispersion relation. They did this

analysis on time - latitude data for 25°, 30°, 35° and 40° N, showing that the zonal phase speed decreased with latitude, which is consistent with linear Rossby theory. In addition to examining Rossby dynamics, they also used the GEOSAT data to track specific features that were generated and propagated through the California Current region. They found that these features propagated to the west with speeds of 1-4 cm sec⁻¹. The most interesting observation made concerning these features is that positive and negative anomalies appeared to follow one another in a wavelike fashion. This observation is what lead them to use CEOF's and power spectrum analysis to show that the Rossby wave signal is evident in the SSH signal of GEOSAT data.

Gower [1989] used GEOSAT data to track specific oceanographic features by examining ascending tracks in the Gulf of Alaska for the period November 1987 to June 1989. In the data set he was able to observe several mesoscale sea level anomalies. Several of these were anti-cyclonic eddies. More eddies appeared to form in the northern part of his domain than in the southern part, which is in the transition region mentioned previously. Most of the eddies observed propagated to the west with speeds between 1 and 2 cm sec⁻¹. A very prominent eddy was observed in the region where the "Sitka" eddy forms [*Kirwan et al.* 1978 and *Tabata* 1982]. *Gower* concludes from this study that SSH anomaly analysis, using GEOSAT, for the Gulf of Alaska region is a significant improvement over that previously supplied by ship data. This is primarily due to the vast improvement in spatial and temporal coverage provided by a satellite. The reader is again referred to the *GEOSAT Special Issue of JGR 1990*, as there are several

papers covering a myriad of topics using GEOSAT data presented there. In summary GEOSAT has proven, and will continue to do so, the value of using radar altimetry for doing oceanographic research.

3. GEOSAT Data and Analysis Methods

3.1 GEOSAT DATA

The data used for this research are organized in two different ways. The first data, which covers the region bounded by the North American coastline west to 150°W and from 20°N to 60°N, are samples from the ERM which have been binned in 1°-latitude by 2°-longitude boxes. The second data are collinear (alongtrack) samples taken from individual satellite tracks which cover a portion of the Gulf of Alaska. The second data are also from the ERM. The data sets cover the entire ERM which lasted from November, 1986 to January, 1990.

3.1.1 Binned GEOSAT Data

The binning of GEOSAT data into the 1° by 2° boxes is accomplished in the following manner. Each altimeter cycle that passes through a given 1° by 2° region contributes a discrete height measurement as a function of time. This measurement is an estimate of an average SSH along the ground track segment that passes through the box. For boxes that have multiple cycles, the measurement for each pass is collected with the others to form an average SSH for the entire box. This average SSH is considered to be located at the center of the box. For the ERM each box is sampled by to form an average SSH for the entire box. This average SSH is considered to be located at the center of the box. For the ERM each box is sampled by

the satellite 2 to 4 times in each 17-day period [*Cheney, 1989*].

The binned GEOSAT data were received with the corrections and adjustments listed in Table 1. Note specifically that the water vapor correction for these data is derived from the FNOC water vapor model since the data set was received prior to the implementation of the SSM/I water vapor corrections. The use of the FNOC water vapor correction may have enhanced or suppressed some of the oceanographic features in the region thus giving a false representation of the sea surface. Also note that there is no inverse barometer correction in this data set.

Since the data received have had a one year mean (August 1987 - August 1988) removed, the data for each bin are a time series of sea level anomalies, spaced on average 17-days apart. After examining the distribution of SSH in the data, it was decided to remove all values greater than 5 standard deviations from the mean. This value was chosen rather than the usual 3 standard deviations because in the northern part of the data domain the SSH variability was very high compared to the southern part. If 3 standard deviations were used than a good deal of the sea surface signal in the Gulf of Alaska would have been removed. This had little adverse affect on the rest of the data set. Less than 0.5% of the data which fell greater than 3 standard deviations from the mean fell less than 5 standard deviations away.

The second step in this analysis was to interpolate between the 17-day points in time and to fill missing blocks of data. This was accomplished with a simple linear interpolation scheme. The data set used begins points in time and to fill missing blocks of data. This was accomplished with a simple linear interpolation scheme. The data set used begins December 15, 1986 and ends June 1, 1989. The reason so much data were

Table 1: List of corrections and adjustments which were made to the binned GEOSAT data [*Cheney, et al. 1987*].

Correction	Source
1. Solid Earth Tide	Model
2. Fluid Tide (Ocean Tides)	Model
3. Ionospheric Correction	Model
4. Wet Troposphere	FNOC Model
5. Dry Troposphere	FNOC barometric pressure
6. Geoid	Model
7. Electromagnetic Bias	Empirical
8. Orbit Error	Quadratic Polynomial

removed at the end of the mission was that there were large data gaps for the region during the last 8 months of the ERM. These large data gaps were due in part to tape recorder failure on the satellite and also spacecraft attitude variability. The latter being caused by increased solar activity in 1989 and by systematic deviations of the satellite [Doyle *et al.* 1990].

The next step in the analysis was to pick an appropriate smoothing routine that would filter out the high frequency signals, which were not of interest in this study. The technique chosen was a 1-2-1 Hanning window repeated 92 times in time to filter signals with a frequency higher than 55-days. The frequency response function for this filter (Figure 6) was chosen to retain Rossby wave propagation and mesoscale features which persist two months or longer. The data were also smoothed in space with a Hanning window once in each of the latitude and longitude directions. This was done to eliminate the 2Δ spatial noise which is a remnant of the binning process. The data were now a smooth 900-day time series of SSH at each 1° by 2° box.

3.1.2 Collinear Track Data

The second data set used in this study consisted of a number of descending and ascending tracks which crossed a portion of the Gulf of Alaska. This data set included all of the corrections and adjustments as the binned data except for a few changes. First, the water vapor correction is derived from the SSM/I; second, a better orbit correction has been included and third an inverse barometer correction has been included is derived from the SSM/I; second, a better orbit correction has been included and third an inverse barometer correction has been included

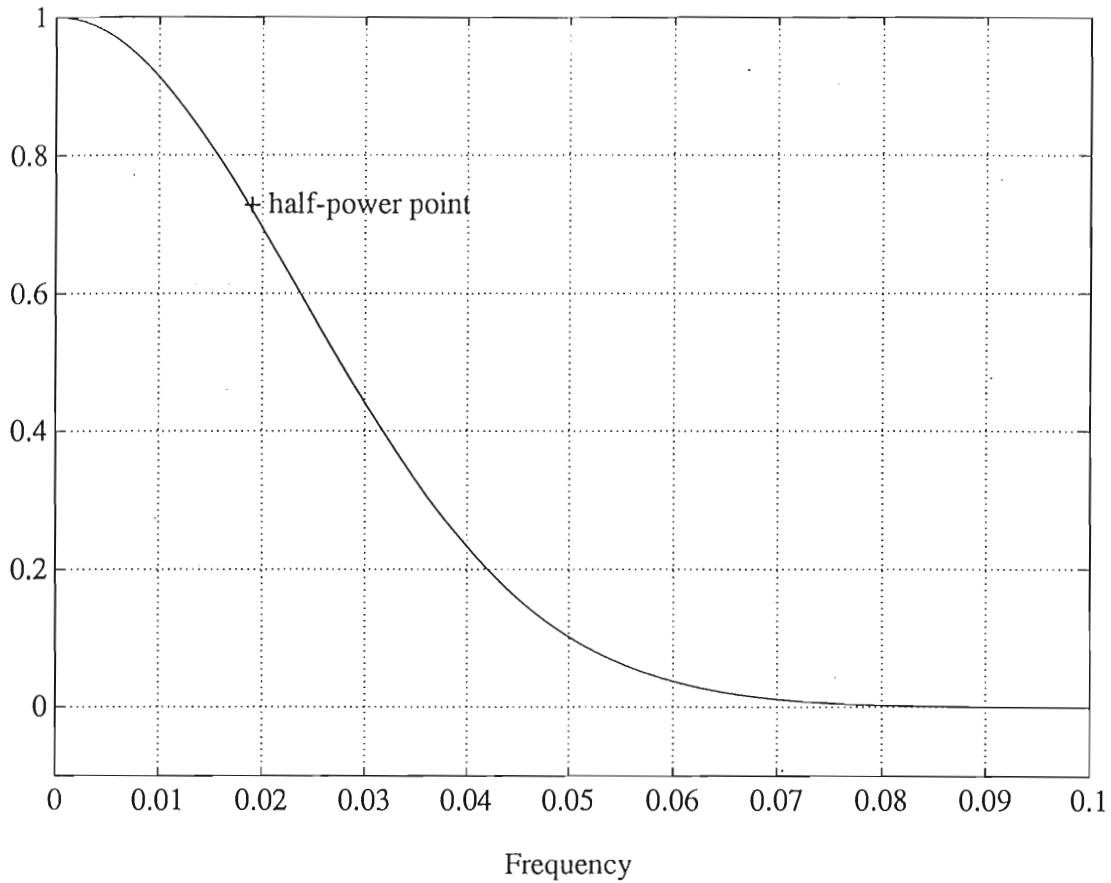


Fig. 6. The frequency response function of the Hanning window used on the binned GEOSAT data. There were 92 passes made in time producing a half-power point corresponding to a period of 55-days. This value was chosen to retain Rossby wave dynamics and mesoscale features which persist two months or longer.

[personal communication with *L. Miller*, 1991]. The descending tracks cross the domain from the northeast to southwest starting at the Pacific coastline of Canada and Alaska. The ascending tracks cross the domain from southeast to northwest starting at the Pacific coastline of Oregon and Washington. Each groundtrack is repeated every 17-days. In some cases there is only a portion of all possible data along a given groundtrack cycle. For extreme cases, no data for a given groundtrack cycle through the domain were available, particularly for the descending tracks. As the satellite transitioned from the polar regions over Canada to the Pacific ocean, the spacecraft attitude did not allow the satellite to send and receive radar pulses to and from the ocean in a straight path. The satellite essentially wobbled when coming across Canada. Until it stabilized along each groundtrack, no SSH data were recorded [personal communication with *L. Miller*, 1991].

The data along each groundtrack are spaced approximately 6.7 km apart, since 10 measurements per second are averaged into a single SSH for each second along track. The spacing is variable, and these variations are caused by such things as high sea state and less than 10 measurements per second, among other reasons [personal communication with *L. Miller*, 1991]. In order to get evenly spaced data along track, a cubic spline with a spacing of 5 km between data points was applied to each cycle of each track. For ascending tracks, when large blocks of data were missing on a given cycle and to avoid extrapolation of data, a filling procedure in time was performed. This technique used an average of the missing value's nearest cycle and to avoid extrapolation of data, a filling procedure in time was performed. This technique used an average of the missing value's nearest neighbors, one forward and one backward in time. For any given

ascending track, there were never more than two consecutive missing cycles. This scheme was not used on descending tracks because there was an excessive amount of missing data in time. Occasionally several consecutive cycles on a given descending track would be missing.

3.2 Data Analysis Techniques

3.2.1 Complex Empirical Orthogonal Functions

The use of CEOF's has been a very successful technique in the analysis of many different kinds of oceanographic and meteorologic data [Shriver *et al.*, 1991, White *et al.*, 1990, White *et al.*, 1987, Barnett, 1983 and others]. The objective of this technique is to extract information about propagating physical features from a space - time data set. This is essentially accomplished by transforming the original data matrix with the Hilbert transform, creating a new complex data set with the Hilbert transform as the complex part, and performing eigenmode decomposition of the new data matrix. As this new matrix is Hermitian, its eigenmodes contain phase and amplitude information about the principle components of the original data. White *et al.* [1987], and Barnett [1983] present a detailed discussion of this technique. A brief review will be presented here.

Let \mathbf{D} be a data matrix with time rows and space columns. Let \mathbf{E} be the Hilbert transform and form:

$$\mathbf{W} = \mathbf{D} + i\mathbf{E} .$$

Compute $\mathbf{W}\mathbf{W}^T$. to obtain a modified covariance matrix $\mathbf{H} = \mathbf{W}\mathbf{W}^T$

$$\mathbf{W} = \mathbf{D} + i\mathbf{E} .$$

Compute $\mathbf{W}\mathbf{W}^T$, to obtain a modified covariance matrix, $\mathbf{H} = \mathbf{W}\mathbf{W}^T$ (where T denotes complex conjugate transpose).

Let \mathbf{A} be a square matrix containing the right eigenvectors of \mathbf{H} and \mathbf{B} be a diagonal matrix containing the eigenvalues of \mathbf{H} . From \mathbf{B} we can find the percent variance of each eigenmode by dividing each eigenvalue by the trace of \mathbf{B} . Depending on whether \mathbf{H} is the temporal or spatial covariance matrix, the individual eigenvectors of \mathbf{A} are the temporal or spatial patterns of each eigenmode. By multiplying \mathbf{W} with the individual eigenvectors of \mathbf{A} , the spatial or temporal patterns can be found.

The most important aspect of CEOF's, which can not be produced by using traditional EOF's, is that amplitude and phase information about propagating features of each eigenmode can be calculated. Recall that phase speed c , is related to the frequency, ω , and wavenumber, k , of a travelling wave by $c = \omega/k$.

Where:

$$\omega = -\frac{d\phi}{dt} \quad \text{Eq. 4.}$$

$$k = \frac{d\theta}{dt} \quad \text{Eq. 5.}$$

The phase, ϕ , of the temporal pattern of the eigenmodes, is the arctangent of the ratio of the imaginary part and the real part of the temporal pattern; i.e. $\phi = \arctan(t_{Im}/t_{Re})$. The phase, θ , of the spatial pattern of the eigenmodes, is the arctangent of the ratio of the imaginary part and the real part of the spatial pattern; i.e. $\theta = \arctan(s_{Im}/s_{Re})$.

The phase, θ , of the spatial pattern of the eigenmodes, is the arctangent of the ratio of the imaginary part and the real part of the spatial pattern; i.e. $\theta = \arctan(s_{Im}/s_{Re})$.

The matrix manipulations were tested on a cosine wave, $D(t_{time}, x_{space}) = A \cos(kx - \omega t)$. The first CEOF eigenmode accounts for

100% of the variance of these data, since the wave form is a "perfect" wave with no noise. This tested technique of calculated CEOF's has been applied to the binned GEOSAT data.

3.2.2 Two-Dimensional Spectral Analysis

White et al. [1990] used CEOF analysis on GEOSAT data in the California Current region. They found that this type of analysis suggests the evidence of Rossby wave propagation in the GEOSAT data but that there was very little quantitative information about the phase speed and direction of the propagating features. Therefore, they used two-dimensional spectral analysis. They chose east-west wavenumber and frequency as the independent variables of this analysis. A brief review of the technique is presented here. The space time data are first transformed into Fourier space using a two dimensional FFT algorithm. The spectrum of these data are calculated. This yields frequency information on the domain $-\frac{1}{2\Delta t} \leq f < \frac{1}{2\Delta t}$, and wavenumber information on the domain $-\frac{1}{2\Delta x} \leq k < \frac{1}{2\Delta x}$. Because the information in negative frequency space is redundant to that in the positive frequency space, the quadrants with negative frequency can be disregarded. This is not the case for the negative wavenumber space. Negative wavenumber reveals information concerning negative (westward) travelling waves.

4. Results

4.1 Visual Analysis of Binned GEOSAT Data

In this age of high speed computers with massive storage mediums and high quality graphics capabilities, it is now possible to produce pictures of the vast quantities of geophysical data provided to us by satellites. Taking the graphics capabilities one step farther, we can animate time series of that data in such a way that we can actually see what the satellites have measured. As it is impossible in a paper of this type to show the animation of the GEOSAT data we have examined, we will make an attempt to describe what we have seen with words. A videotape of the animated GEOSAT data is available upon request from the author. Visual analysis of the GEOSAT SSH for the region depicted in Figure 1 provides a good starting point to identify mesoscale features. Identified mesoscale features can indicate the path to more concentrated study of specific features within the region. Many of the specific features observed in the animation process warrant discussion.

One of the most prominent features in the SSH is the annual signal. Each winter in the three year data set shows the same general pattern as any other, and the same is true for the summer pattern. Westward propagation of sea-level anomalies is evident throughout the data set, any other, and the same is true for the summer pattern. Westward propagation of sea-level anomalies is evident throughout the data set,

suggesting the evidence of Rossby wave dynamics. This is especially true in the southern portion of the data domain. Propagation of anomalies is also evident along the coastline of North America. The evidence of this is very segmented and sporadic. Poleward Kelvin wave propagation in this region has been shown to exist (*Pares Sierra and O'Brien, 1989*), and is therefore expected to be found in the GEOSAT SSH.

Seasonal upwelling and downwelling are both evident along the coasts of California, Oregon, and Washington. Coastal propagation of sea level anomalies is especially evident in the Gulf of Alaska. This is strong evidence of the seasonal and interannual intensification and relaxation of the Alaska Current and the Alaskan Stream.

In the region about 5° to the north and south of 45°N occasional eastward propagation of sea level anomalies is observed. As shown previously, the mean flow pattern at this latitude is towards the east. This eastward surface flow is the manifestation of the West Wind Drift and Subarctic Current. Because the mean SSH has been removed from this data set only anomalies of the flow of these two currents is evident in the sea level signal. When these flows meander, or are intensified or relaxed from the mean, an SSH anomaly should be evident. These features are then transported to the east by the mean surface flow until they reach the transition region near the coast. Once they reach this transition region, it is very difficult to see the direction of propagation they assume at that point. In general, the transition region is in a very confused, state but at times there is evidence that westward propagation does occur out to about ten
In general, the transition region is in a very confused, state but at times there is evidence that westward propagation does occur out to about ten

degrees from the coastline. Just to the south of this region right along the coast, there is evidence of the winter formation of the Davidson current.

One very prominent feature in the southeastern part of the domain will only be mentioned in passing, as this research concentrates on the Gulf of Alaska. In the fall of 1987, there is an intense positive sea level anomaly which forms along the coast of Baja California and propagates to the west. The timing for this event suggests that it may be related to the 1986 - '87 equatorial El Niño event. *Norton et al.* [1985] present results of several studies that indicate that there is an oceanographic response, in the form of positive sea level anomalies, to equatorial El Niño events in the Baja region. This response is delayed from 8 to 10 months after the equatorial event. The most striking example of this was the 1982 - '83 El Niño which produced a very strong coastal warming signal in the fall of 1983. Warm anomalies of ocean temperature at the surface is reflected in the SSH as a positive sea level anomaly. The positive sea level anomaly observed in the fall '87 GEOSAT data is consistent with the *Norton et al.* observations.

4.2 CEOF Analysis of Binned GEOSAT Data

As described in the previous section, a useful technique for isolating propagating features in a two dimensional data field is that of CEOF's. Here we are interested in isolating westward propagating features in the region from 40°N northward into the Gulf of Alaska. One of the objectives is to compare results from this analysis of GEOSAT data with data produced region from 40°N northward into the Gulf of Alaska. One of the objectives is to compare results from this analysis of GEOSAT data with data produced by reduced gravity, baroclinic models of the same region. As *White et al.*

[1990] employed the same basic analysis techniques in the California Current region, including 40°N , we begin our analysis at 45°N .

At 45°N a space - time data matrix (from 125°W to 137°W) of the 900-day GEOSAT data set was constructed in order to perform the CEOF analysis. Due to a great deal of unresolvable interannual variability in this data matrix, very little useful information was extracted from the initial CEOF analysis. In order to eliminate the unresolvable low frequency signal, the data were averaged into a composite one year data set (Figure 7). It is readily apparent that there is westward propagation of sea level anomalies at this latitude. It is also obvious that there is a strong annual signal in the data. The sea level at the eastern edge of the domain is lower than the mean in the winter and higher than the mean in summer. The CEOF of this composite data set was calculated yielding some interesting results.

The first CEOF mode accounts for 88% of the variance of SSH. We assume the remaining variance is noise; therefore, only the first mode will be discussed here. In the temporal pattern (Figures 8a & 8b) of the first eigenmode, the annual signal is obvious. There is a negative phase shift between the real and imaginary components of the temporal pattern. The real and imaginary components of the spatial pattern (Figures 8c & 8d) also show a phase shift, but otherwise show little information about the data. A more interesting and informative representation is one of the amplitude of the spatial pattern (Figure 9). This shows that the maximum variability of SSH occurs near 127°W which is approximately 235 km from the coast of the spatial pattern (Figure 9). This shows that the maximum variability of SSH occurs near 127°W , which is approximately 235 km from the coast of North America. Using the relationships between the spatial phase

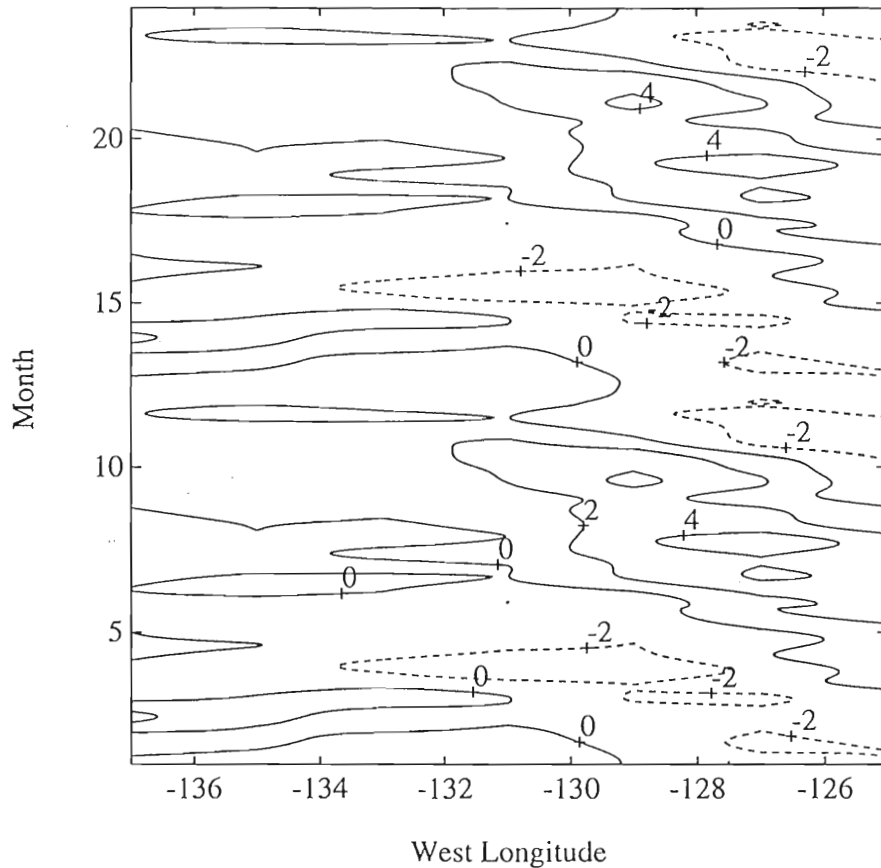


Fig. 7. Composite of GEOSAT SSH data at 45°N , 125°W to 137°W . Two years are shown to emphasize the annual signal. Notice that the maximum variability is in the eastern part of the data domain. Note also that there is a sloping pattern directed towards the upper left part of the plot. This indicates that as sea level anomalies form near the coast they propagate to the west in time. The SSH contours are in centimeters and negative values are dashed.

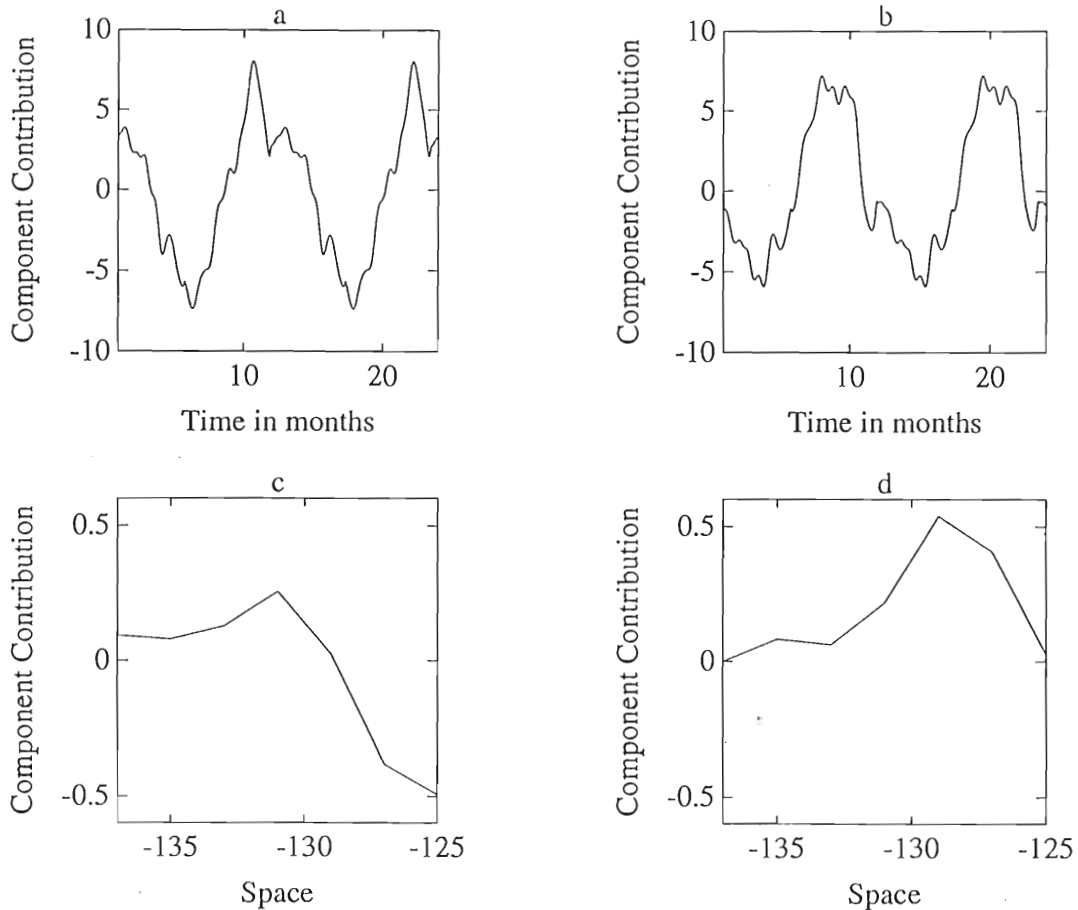


Fig. 8. First eigenmode at 45°N accounting for 88% of sea level variance. The time axis is in months with month 1 and 13 corresponding to January. The spatial axis is in degrees longitude. a) & b) Real and imaginary components of the temporal pattern. Notice the strong annual signal and the phase shift between the real and imaginary components. c) & d) Real and imaginary components of the spatial pattern. Again note the phase shift between the two components.

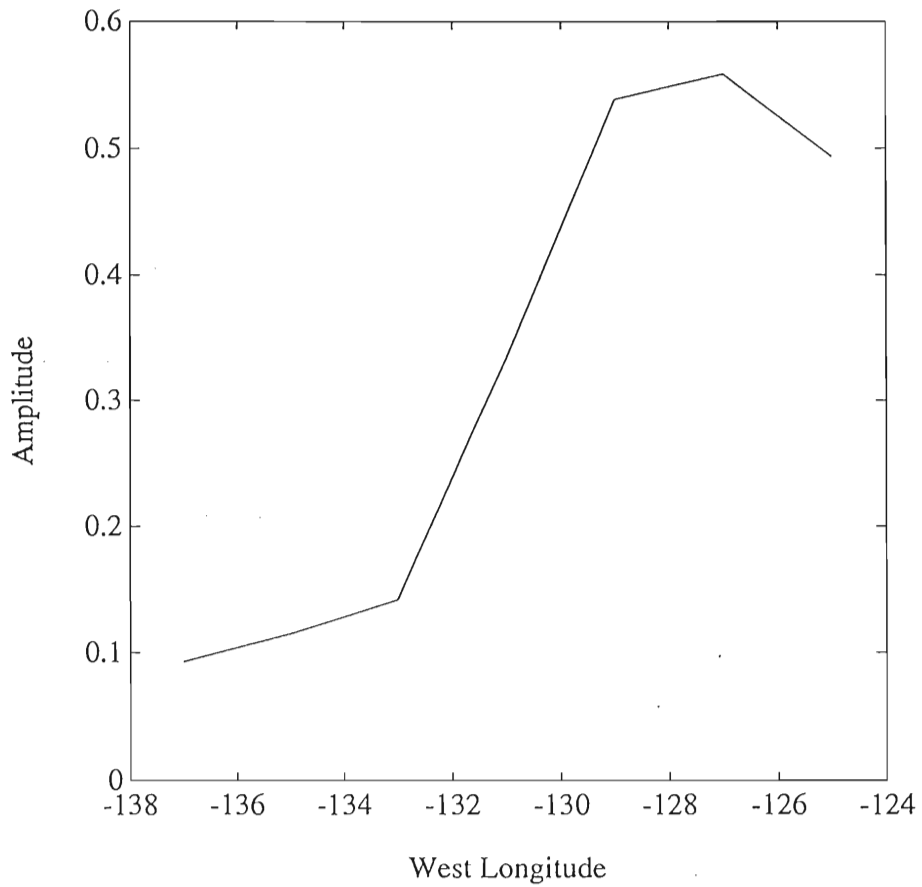


Fig. 9. The amplitude of the spatial pattern of the first eigenmode at 45°N

Fig. 9. The amplitude of the spatial pattern of the first eigenmode at 45°N. Notice that the maximum variability is at approximately 127°W and that the variability of sea level is greatly reduced well offshore.

function and wavenumber, and the temporal phase function and frequency, a phase speed and direction of the propagating features can be calculated. The temporal and spatial phase functions were calculated and as they had near constant rate of change a straight line was fit to each to calculate their derivatives. From the method previously described, a mean phase speed of -4.0 cm s^{-1} was calculated. The negative value implies westward propagation along 45°N . As this speed is higher than the theoretical Rossby wave speed for this latitude we can not conclude that the westward propagation of sea level anomalies is due to Rossby wave dynamics.

A space time picture of the first eigenmode (Figure 10) (reconstructed from the temporal and spatial patterns) shows several very noticeable features. First, as observed in the amplitude of the spatial pattern, the maximum variability occurs at around 127°W . Initially it was expected that the maximum variability of GEOSAT SSH would be present at the coast for this latitude. This proved not to be an incorrect assumption, but one which GEOSAT could not verify because the satellite did not measure sea level right along the coast. Due to the nature of the binning process any data recorded within 2° of the coastline at 45°N shows up as a value at 125°W . For that reason and because the satellite generally does not acquire the sea surface until some distance from the coastline, there is no accurate representation of coastal sea level in GEOSAT SSH. This makes the task of verifying GEOSAT data difficult because coastal tide gauge data can not be used. The second feature observed in the first eigenmode is between 125°W and about 130°W . Here, the sea level anomalies are positive in the winter and negative in the summer. The second feature observed in the first eigenmode is between 125°W and about 130°W . Here, the sea level anomalies are negative in the winter and positive in the summer. This agrees with steric height calculations

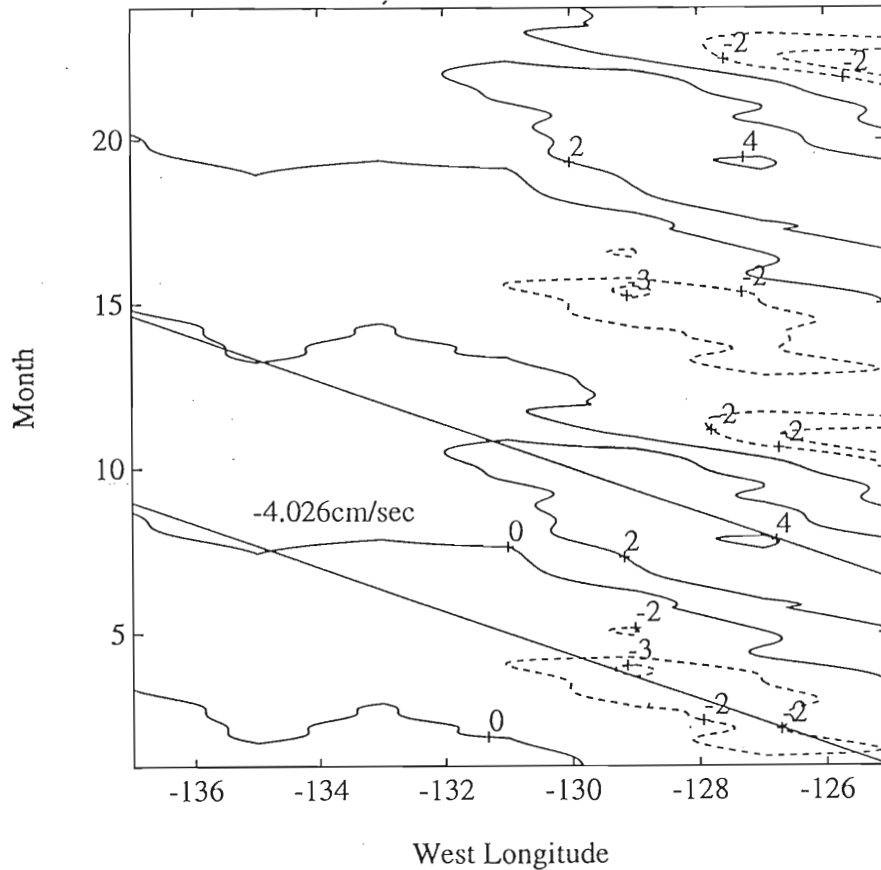


Fig. 10. Reconstructed contour of the first eigenmode at 45°N . This picture is produced by combining the temporal and spatial patterns of the first eigenmode. As shown in the spatial pattern, the maximum variability of sea level occurs around 127°W . The annual signal is quite evident, with sea level near the coast being negative in the winter and positive in the summer. For reference purposes the calculated average phase speed is superimposed on the contour of sea level.

made by *Huyer* [1977]. She shows that the steric height at 300 km (about 128°W) offshore is least in late winter and greatest in summer. This is a result of the seasonal heating and cooling cycle. The associated sloping pattern (less negative anomalies in winter and less positive in summer) towards the coast is an indication of the formation of the Davidson current in the winter and its disappearance in summer. The westward propagation of sea level anomalies is strongest from 125°W out to 132°W. This observation is in agreement with the numerical study of *Pares-Sierra and O'Brien* [1989], which will be discussed in more detail in the next section. West of 132°W the variability of sea level is very low in amplitude again in agreement with *Pares-Sierra and O'Brien* [1989]. For reference the calculated phase speed from the CEOF analysis is shown superimposed on the contours of SSH. Notice that some features appear to travel faster than the calculated phase speed, while others travel slower.

Progressing northward into the Gulf of Alaska the same analysis technique was performed at 49°N. The data prior to processing are shown in Figure 11. A very distinct difference between the data at this latitude and that of 45°N is that the amplitude of the SSH variability is smaller. The first eigenmode of this spatial series accounted for 66% of the variance. Its temporal and spatial patterns are shown in Figure 12, with the following interpretation. As at 45°N an annual signal is observed in the temporal pattern. The amplitude of this signal is not as large and there seems to be more shorter time scale variability superimposed on the annual signal, at this latitude. The spatial pattern is very similar to that at 45°N, but again more shorter time scale variability superimposed on the annual signal, at this latitude. The spatial pattern is very similar to that at 45°N, but again the amplitude of this pattern is more interesting (Figure 13). The

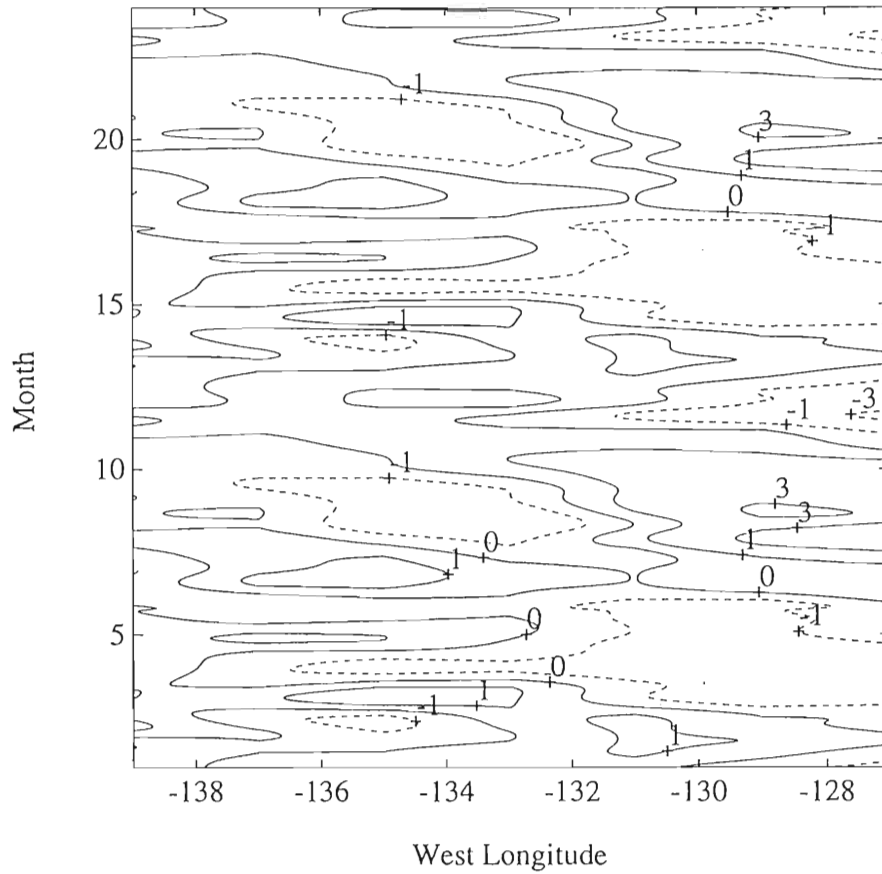


Fig. 11. Same as Figure 7 but for 49°N. Notice that the amplitude of the

Fig. 11. Same as Figure 7, but for 49°N. Notice that the amplitude of the SSH is smaller at this latitude.

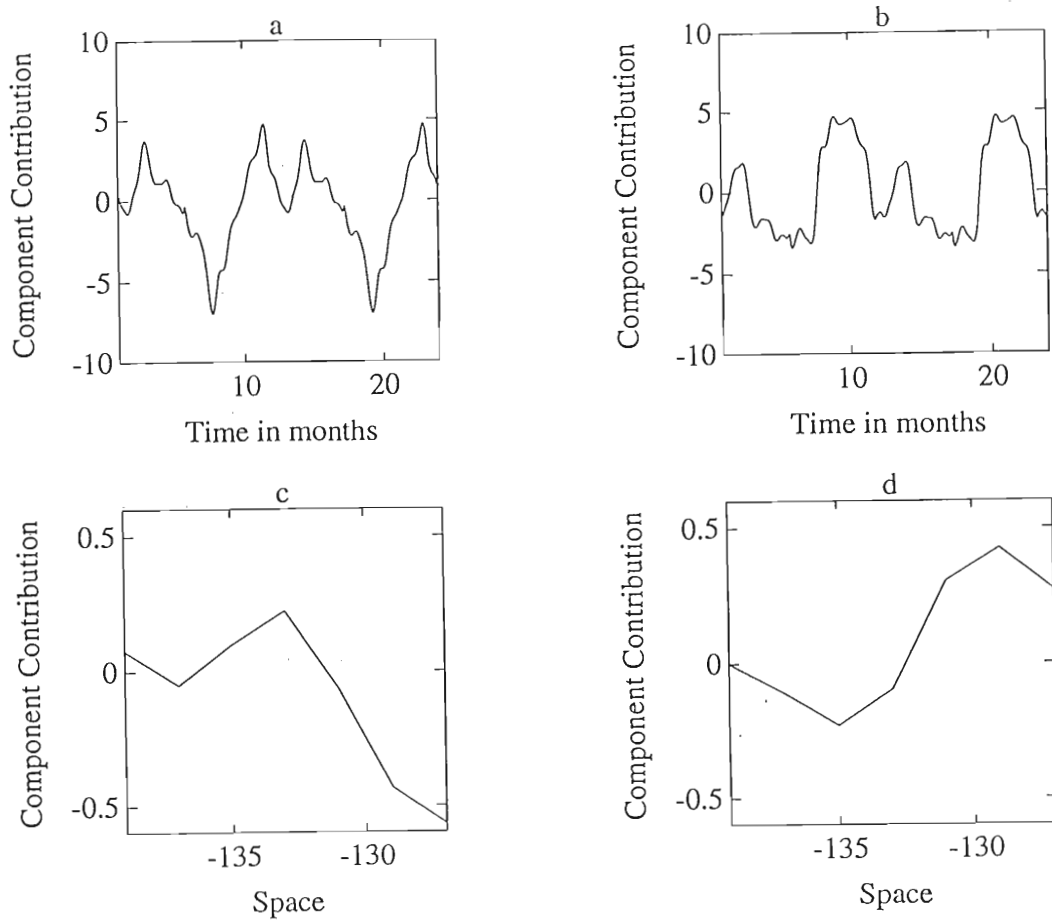


Fig. 12. Same as Figure 8, but for 49°N . Notice that in the temporal pattern

there is more shorter scale variability observed than at 45°N .

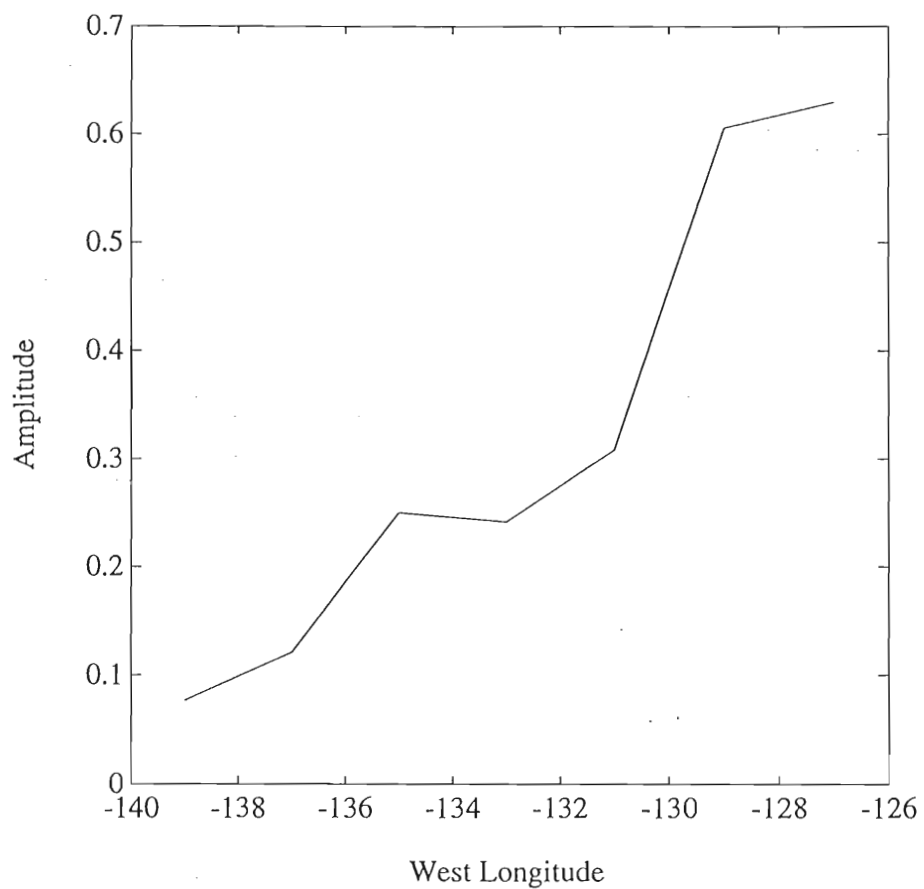


Fig. 13. Same as Figure 9, but for 49°N. The most interesting difference of the amplitude at 49°N, compared to 45°N, is that the maximum variability

Fig. 13. Same as Figure 9, but for 49°N. The most interesting difference of the amplitude at 49°N, compared to 45°N, is that the maximum variability occurs closer to the coast.

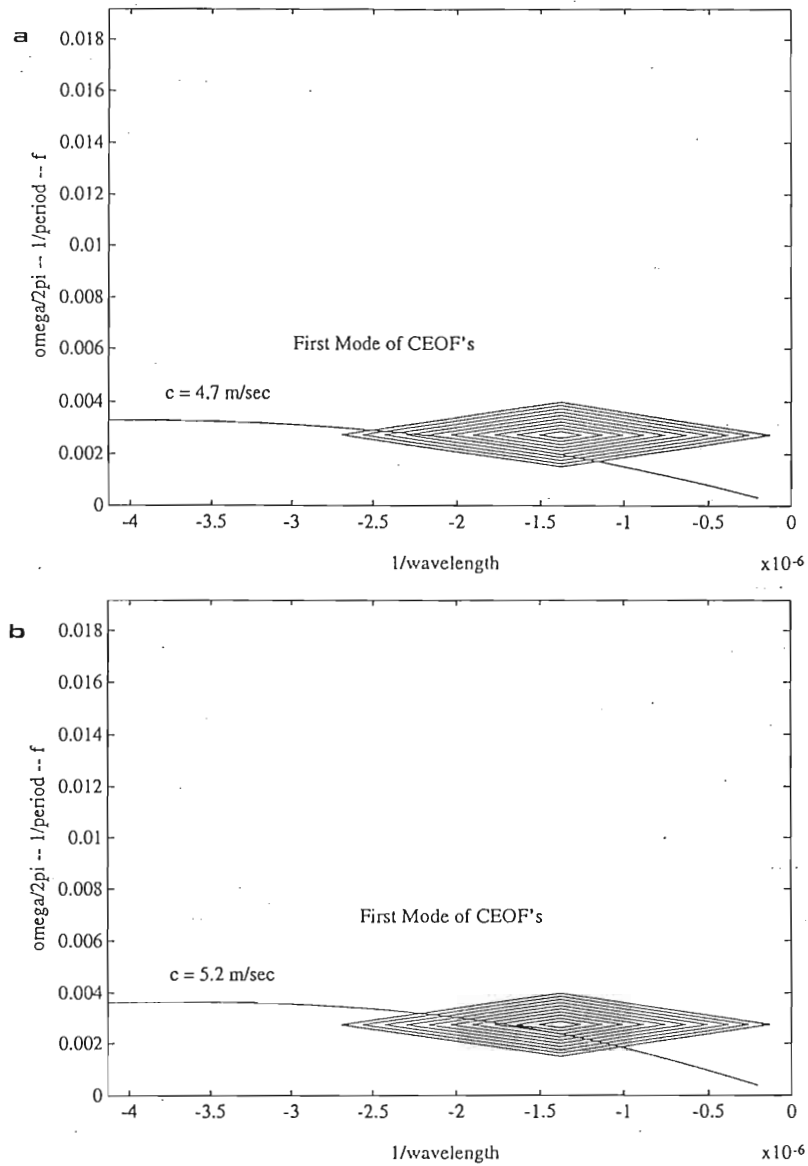


Fig. 20. Same as Figure 19. but for 57°N . Also the value of c has been

changed to a) 4.7 m s^{-1} and b) 5.2 m s^{-1} .

4.4 Analysis of Collinear GEOSAT Data in the Gulf of Alaska

In an effort to examine the variability of sea level on shorter time and smaller spatial scales than those studied using the binned GEOSAT data, SSH data from independent ascending and descending tracks has been analyzed. Ascending satellite tracks traverse the region of study from the southeast to northwest, while the descending tracks traverse the region from the northeast to southwest. It was found that for the entire GEOSAT mission much of the SSH data from the descending tracks was unusable due to satellite instabilities. This is in agreement with *Gower's* [1989a & b] study utilizing a smaller data set in time (November, 1986 to June, 1988). Due to this problem only ascending tracks will be discussed in this analysis. Three ascending tracks have been examined to find out how sea level anomalies travel when generated near the coast of Alaska and British Columbia. Using the numbering system described by *Gower* [1989a & b] we examine ascending tracks 171 - 173 (see Figure 21). One of the primary motivations for this particular analysis is to compare the near coast, sea level signal as measured by GEOSAT to the near coast signal of a reduced gravity baroclinic model which will be discussed in the next section.

The data for the three tracks are shown in Figures 22 - 24. Track 173, which is the closest track to the coastline contains some very interesting features. As observed by *Gower* [1989a & b] it is obvious that there are many sea level anomalies with spatial scales on the order of 100 to 200 km, and spatial scales of a few months to several months. The northwestern end of sea level anomalies with spatial scales on the order of 100 to 200 km, and spatial scales of a few months to several months. The northwestern end of the satellite track appears to be the most energetic in the sense that the

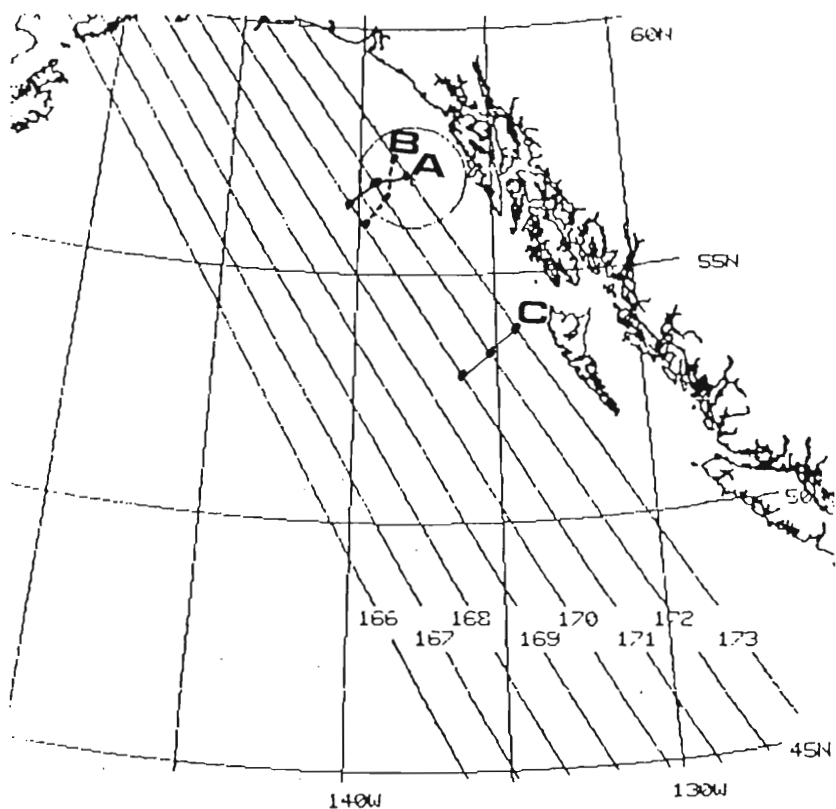


Fig. 21. The region of study showing the selected ascending tracks used in examining the sea level variability along the Alaska and British Columbia coastlines. The three features "A", "B", and "C", are marked to show the westward propagation of sea level anomalies and are discussed in the text. The track numbers are as described by Gower [1989a & b].

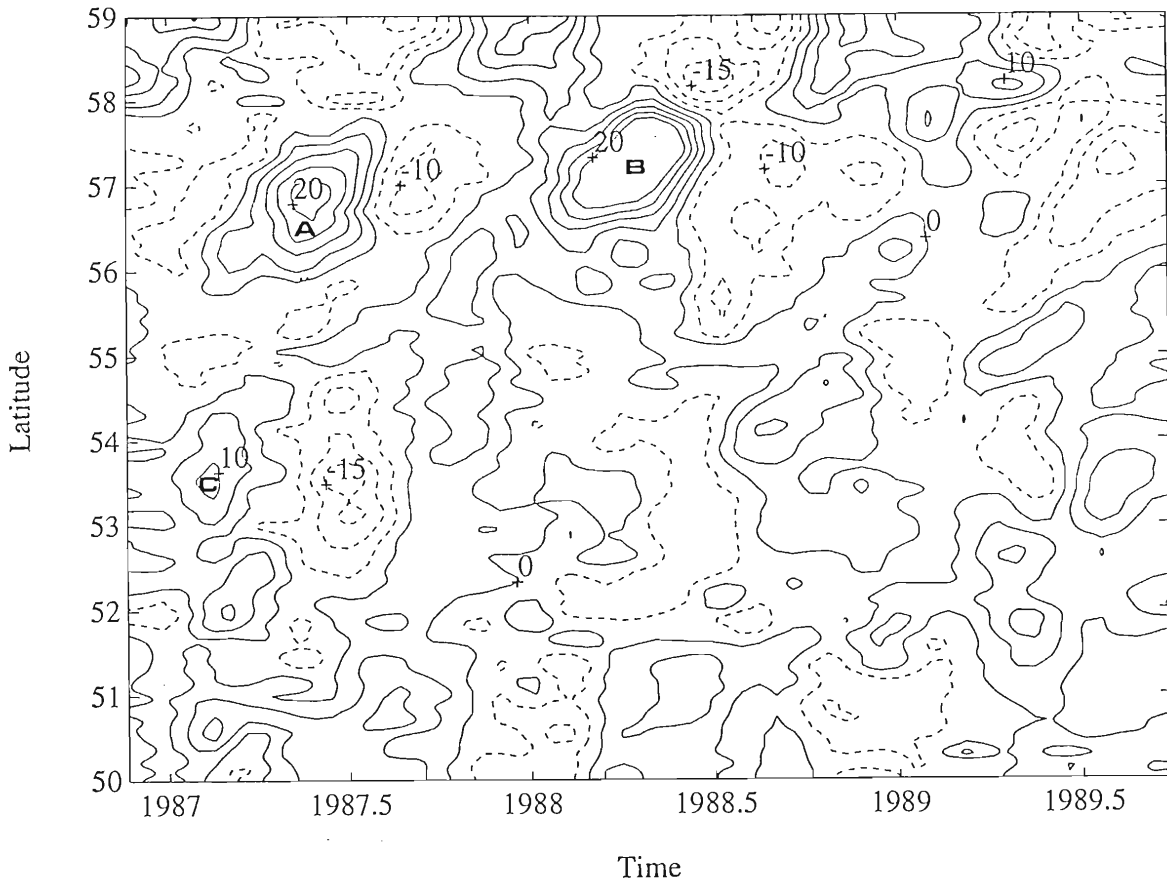


Fig. 22. A time/latitude contour of ascending track 173. This track is the closest complete ascending track to the coastline. The data points are separated by 5 km in space and 17-days in time. The contour interval is 5 cm. Notice that there are several eddy like features in addition to those that are marked. A particular area of interest is at the northern part of the track. A considerable amount of variability is evident on the annual time scale in this segment of the track. This is evidence of the seasonal variability of the coastal current in this region.

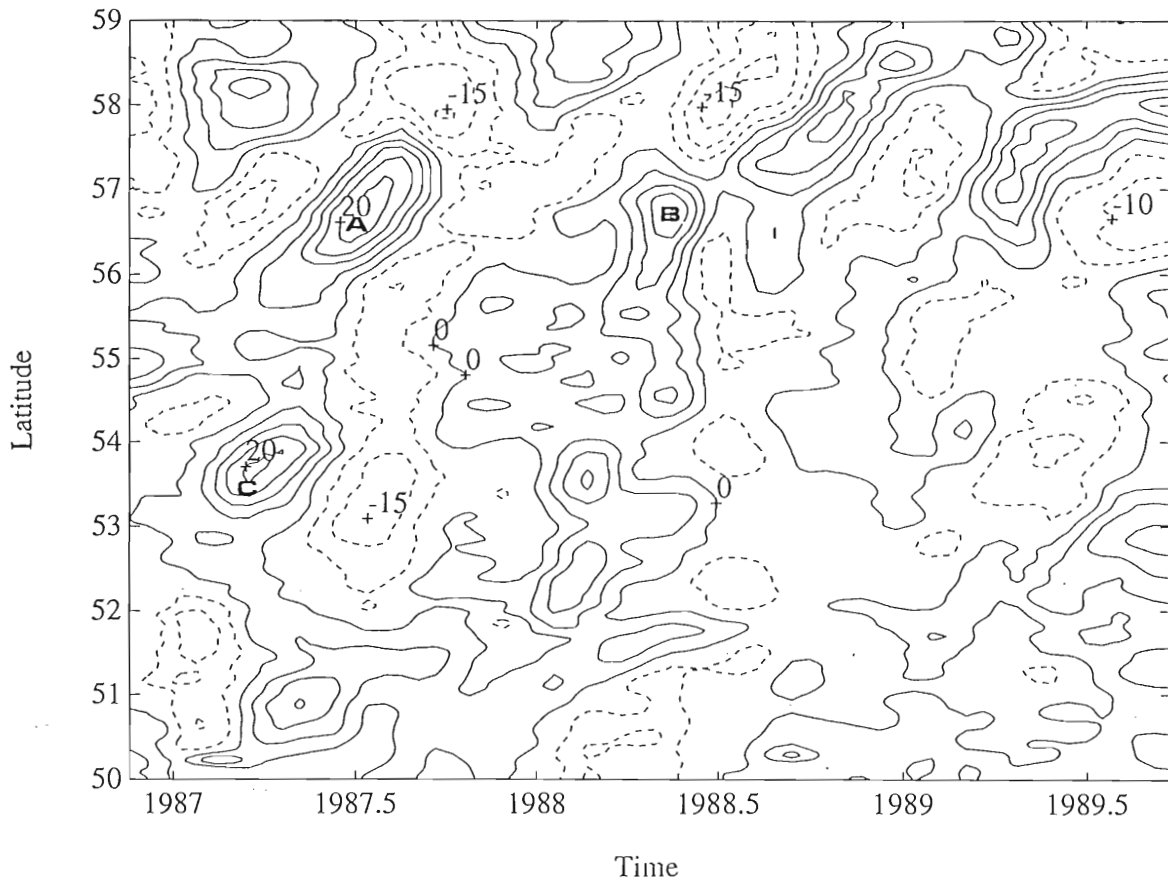


Fig. 23. Same as Figure 22, but for track 172.

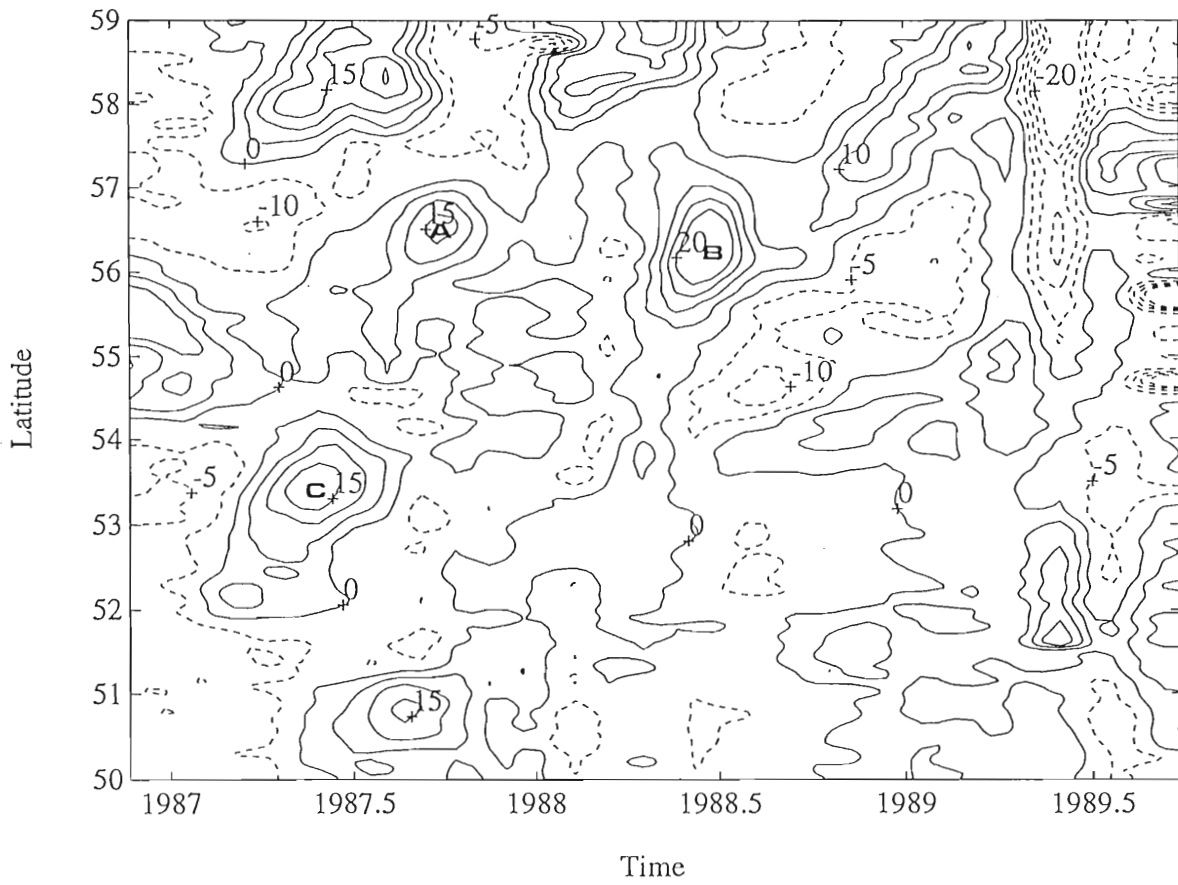


Fig. 24. Same as Figure 22 and 23, but for track 171.

variability of sea level is more intense here. Two very noticeable positive anomalies (first observed by *Gower* [1989a]) are located near 57°N and 138°W. This is the location of the recurring Sitka eddy first described by *Tabata*, [1982]. The intensity and duration of this eddy is significant in that it greatly affects the coastal circulation in this region. One result of this is that salmon migration routes may be altered by this feature (see *Hamilton and Mysak* [1986]).

The first time that the eddy is seen along this track is in the late winter, early spring of 1987 (feature "A" in Figures 22 - 24). It persists well into the summer of that year. The size of the eddy at its maximum diameter as seen by track 173 is on the order of 200 - 300 km. This occurs in May of 1987. The eddy is again seen to form in February of 1988 and persist until at least June of the same year (feature "B"). *Gower* [1989a] uses the argument that the negative sea level anomaly is a remnant of the removal of the mean sea surface and not the reversal of the eddy. If true then the eddy actually persists much longer than shown in the contour. Again the maximum diameter of the eddy is on the order of 200 - 300 km. The most important new observation, as compared to that of *Gower* [1989a & b], is that the Sitka eddy shows no evidence of forming in the spring of 1989. This agrees with *Tabata* [1982] who found that the eddy does not form every year.

There is a great deal of variability to the north of the Sitka eddy at the annual period. Some of the positive and negative anomalies are very intense. This segment of the satellite track crosses the area where the Alaska Current begins to transition into the Alaskan Stream. *Thomson et al.* [1989] show that this transition is not smooth in nature, and the region

shows evidence of a great deal of variability. The intensity of the sea level anomalies in this region support their conclusion. The anomalies observed in this segment of track 173 are also indicative of the seasonal intensification and relaxation of the coastal currents in the Gulf of Alaska.

To the south of the Sitka eddy, off the coast of the Queen Charlotte Islands, there is evidence of another intense eddy like feature. The positive indication of this feature forms in January of 1987 and by summer of the same year the signal is negative. This feature is labeled "C" in Figures 22 - 24. There is no evidence that this feature recurs in subsequent years. There are several other prominent SSH anomalies along this track which indicates that this region is very energetic.

It is interesting to examine tracks 171 - 173 together to observe westward propagating sea level anomalies that are evident from track to track. The positions along each track of features "A", "B", and "C" are marked in Figure 21. It is readily apparent that the SSH anomalies propagate to the southwest. The positions are plotted along track by subjectively marking the position when the satellite observed the maximum positive amplitude of each feature. By doing this for each of the features on each of the three tracks, an estimate of the speed of propagation can be made. From track 173 to track 171, feature "A" travels at an average speed of 1.74 cm s^{-1} , "B" at 3.53 cm s^{-1} , and "C" at 3.9 cm s^{-1} . This is consistent with the calculations made by *Gower* [1989a & b], and the results that *Cummins and Mysak* [1988] observed from their model analysis of the region. The northern segments of the other ascending tracks show as *Cummins and Mysak* [1988] observed from their model analysis of the region. The northern segments of the other ascending tracks show as much variability as track 173. The main difference being that there is a

time lag from track to track of individual anomalies. This is evidence that the intensification and relaxation of the coastal jet starts in the eastern part of the Gulf of Alaska and progresses towards the west.

5. Comparison of GEOSAT Data to Selected Model Results

As mentioned previously, one of the objectives of this research was to compare GEOSAT SSH to the sea level signal produced by numerical models of the same region. We use 1-1/2 layer, reduced gravity, baroclinic models with bottom topography for this comparison. For complete descriptions of the models see *Pares Sierra and O'Brien*, [1989], *Johnson and O'Brien*, [1990], and *Heim et al.* [1991]. There are two models that overlap the region of the GEOSAT study. The first is a model of the California Current region and extends to 50°N. It is forced by climatologic monthly mean wind stress at the local scale and also has a remote forcing component from coastally trapped Kelvin waves which are produced by a model of the equatorial region of the Pacific Ocean. The second overlaps the first by 5° beginning at 45°N and extends to the coastline of Alaska. It is forced only by climatologic monthly mean wind stress.

We begin by comparing the sea level signal as seen by GEOSAT at 45°N to the Upper Layer Thickness (ULT) produced by the California Current region model. In Figure 7 of their paper, *Pares Sierra and O'Brien* [1989] show the long term monthly ULT anomaly derived from the local forcing mechanisms of their model. Referring to the region from 40°N to 50°N, we observe a very similar pattern to the ULT as we find in GEOSAT SSH. As discussed previously, GEOSAT does not resolve the sea level at 50°N, we observe a very similar pattern to the ULT as we find in GEOSAT SSH. As discussed previously, GEOSAT does not resolve the sea level

signal at the coast, so we turn our attention to 126°W and westward. In the winter, the sea level is characterized by a negative sea level anomaly (see Figure 10). The maximum negative value occurs at approximately 127°W and propagates to the west in time. This is precisely the pattern that the ULT of the model generates. The negative values of ULT (meaning the ULT is thinner than the mean), is manifested in the sea level signal as a negative anomaly. By March of each year, a positive anomaly of sea level starts to propagate into the GEOSAT domain, and we see a positive anomaly of ULT propagating from the coast reaching 126°W . By July the sea level is positive from 126°N all the way to 130°N . Again this is the same pattern that is displayed in the ULT of the model. By late fall the process begins to repeat itself. It is observed in both the GEOSAT data and the model data that the maximum variability occurs around $127^{\circ} - 128^{\circ}\text{W}$. Proceeding westward of 132°W in both data sets, the anomalies are very weak and most generally approach the mean sea level and ULT. *Pares Sierra and O'Brien* [1989] attribute this phenomenon to the existence of the theoretical critical latitude for an annual wave ($\sim 35^{\circ}\text{N} - 40^{\circ}\text{N}$). Their conclusion (supported here by GEOSAT observations), is that south of the critical latitude, waves can propagate to the west as free Rossby waves but north of the critical latitude they present a decaying component.

We now turn our attention to the more recent of the two models in an attempt to verify some of the results it produces. CEOF analysis was performed on a subset of model results in the same manner as that done for the GEOSAT data at 45°N . To prevent any contamination of the results performed on a subset of model results in the same manner as that done for the GEOSAT data at 45°N . To prevent any contamination of the results from the choice of boundary conditions of the model, 46°N was chosen as the

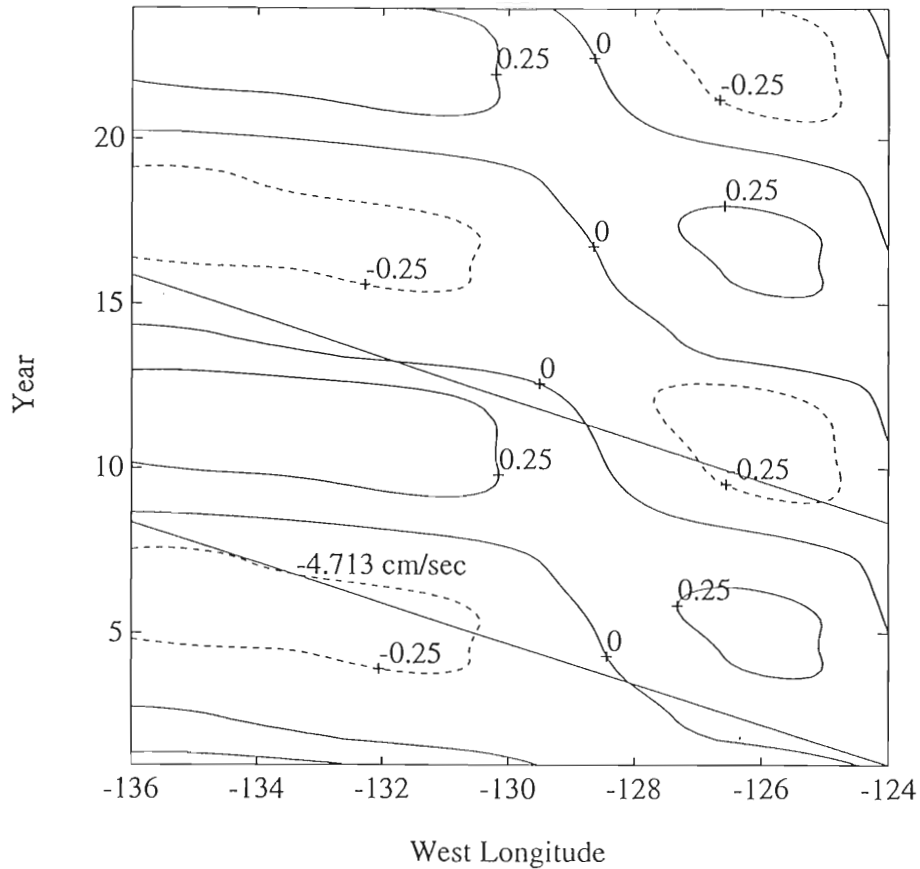


Fig. 25. The combined spatial and temporal patterns of the first eigenmode of the sea level signal produced by the Gulf of Alaska model. An indication of westward propagation of anomalies is observed in the sloping contours as in the GEOSAT data. The mean phase speed of propagation of the model anomalies is faster than the GEOSAT data. Also there is a second area of high variability well offshore which is not evident in the GEOSAT data. The mean phase speed of propagation of the model anomalies is faster than the GEOSAT data. Also there is a second area of high variability well offshore which is not evident in the GEOSAT data. This may be due to the fact that the model only contains a remote forcing component.

line of latitude for this analysis. The first eigenmode accounts for 97% of the variance of the sea level produced by this model. The reconstructed space/time matrix of that mode is displayed in Figure 25. The general structure of the contour plot is the same as that of the GEOSAT data with westward propagation of sea level anomalies being obvious. The calculated mean phase speed is higher in the model than for the GEOSAT data. Also there is a second region of high variability away from the coast, which is not evident in the GEOSAT data. A possible explanation is that this latitude is close to the open boundary of the model. Since the model is forced only with local wind stress, external mechanisms do not influence circulation in the model as they do in the SSH data. Performing CEOF analysis at other latitudes did not yield information that was comparable to the GEOSAT data.

Some of the physical features which are produced by the model and are described by *Heim et al.* [1991] are indeed evident in the GEOSAT data of the region. The most prominent of these features is the propagation parallel to the coastline of sea level anomalies. As discussed in the last section, GEOSAT shows a seasonal signal of the intensity of the coastal jet. This is also a result of the model, however there does seem to be a phase shift between the model data and the GEOSAT data. *Heim et al.* found that this was similarly true when comparing model data to tide gauge data of the same region.

One of the most significant results of the model was the formation of a very intense cyclonic eddy off of the Queen Charlotte Islands. This eddy

One of the most significant results of the model was the formation of a very intense cyclonic eddy off of the Queen Charlotte Islands. This eddy formed in the winter of 1986, 1987, and 1988 and persisted until late spring

of each year. It also formed in early spring of 1989 but was not as intense as in the previous years. It was hoped that by examining the ascending track SSH data over the region that an eddy similar to the one described would be observed in the GEOSAT data. Unfortunately, this was not the case. As mentioned previously, there was an eddy like formation off the coast of the Queen Charlotte Islands in the winter of 1987, but this was anti-cyclonic in nature. Therefore, this feature cannot confirm the existence of the eddy which is produced in the model. In general this model did not produce the number of eddies that routinely are observed in the region. It did produce a small, anticyclonic eddy near the region where the Sitka eddy is known to form, but it was considerably smaller and of less duration than shown in observations. One of the probable causes for the model not resolving the number of eddies expected is due to the absence of baroclinic instability in this model. *Cummins and Mysak* [1988] show in their numerical studies that baroclinic instability is one of the driving mechanisms that produce the numerous eddies in the region. A second possibility, as mentioned by *Heim et al.* [1991], is that the time scale of the wind forcing may not be short enough to induce a large number of eddies.

6. Conclusions

We have shown, that even with its many shortcomings, the GEOSAT satellite rendered a great deal of excellent sea level information about the Northeast Pacific Ocean and Gulf of Alaska. When appropriate time scales are examined, the evidence of westward propagating features is present in sea level anomalies at 45°N. For this study, it was necessary to remove the unresolvable interannual variability in the 2.5 year original record and reduce the data set to a one year composite of all available data. As *Shriver et al.* [1991] have shown in XBT and model data at 40°N, the evidence of such propagation diminishes offshore which they attribute to Rossby wave dispersion and the proximity to the critical latitude of the annual Rossby signal. As we go north into the Gulf of Alaska, we do not find direct evidence of Rossby wave propagation on the annual time scale. This supports that a critical latitude does indeed exist for the annual Rossby wave signal which is generated at an eastern boundary. In the Gulf of Alaska, there is evidence that some mesoscale features do propagate with speeds that are close to the theoretical Rossby wave phase speed. This inconsistency warrants further investigation.

Individual ascending track information along the coast of Alaska and British Columbia was analyzed to examine mesoscale features. This type of data seems to be the most appropriate for examining features on the coast of Alaska and British Columbia was analyzed to examine mesoscale features. This type of data seems to be the most appropriate for examining features on the

order of 100 km and several weeks to several months. We found, as did *Gower* [1989a & b], the formation of the now well known Sitka eddy in the winter of both 1987 and 1988. The eddy did not recur in the winter of 1989. We also show that there are a number of other eddies evident in the GEOSAT data as well as the variability of the Alaska Current and the Alaskan Stream. The ascending track information was very useful in confirming the conclusion made by *Thompson et al.* [1990] that the transition region between these two currents is not smooth as originally presumed.

Because GEOSAT is the first tool which provides a very long term and spatially dense network of sea level data throughout the world's oceans, it has proven itself useful in the validation studies of numerical models. We have shown that the sea level signal as seen by GEOSAT at 45°N is very similar to the yearly anomalies produced by a numerical model of the same region [*Pares Sierra and O'Brien*, 1990]. The GEOSAT results support their conclusions that north of the critical latitude for free Rossby wave propagation the variability of sea level is most likely a result of local forcing. The sea level signal at the higher latitudes is highly correlated on the annual frequency with the wind patterns in the region. We have also shown that it is a good tool for pointing out some of the shortcomings of a numerical model (i.e. the Gulf of Alaska model, *Heim et al.* [1991]).

We feel that as useful as GEOSAT has been in helping scientists to better understand the circulation of the world's oceans, there are some lessons which should be learned from its shortcomings. First, and better understand the circulation of the world's oceans, there are some lessons which should be learned from its shortcomings. First, and foremost, we feel, as do many other altimetry data users, that the next

generation of satellite altimeters must have a means of evaluating directly the effects of water vapor on the path length of each radar pulse. We hope that the instruments that have been developed for ERS-1 and TOPEX will provide this information as required. We also feel that even though the binning process described is adequate for examining large temporal and spatial scale phenomenon, it is unrealistic to take potentially hundreds of observations and average them into a single number and place it at the center of a specified 1° by 2° bin. At the equator, the distance between the center of each bin in the zonal direction is 222 km. Any features that are smaller than this are aliased by the binning process if they lie in between the centers of the bins. On the other hand, the zonal separation of adjacent satellite tracks at the equator is on the order of 150 km, thus providing an increased spatial resolution. As the satellite tracks approach the poles the distance between adjacent tracks is greatly reduced. Currently there is ongoing research at this site to alleviate some of the problems described here by creating a powerful visual data representation package, which will be useful for all types of satellite data.

Analyzing GEOSAT data has emphasized some of the shortcomings of the Gulf of Alaska model. There is currently, or will be in the near future, ongoing research that will attempt to improve the quality of the model results. Initially, baroclinic instability will be allowed by increasing the number of layers from 1-1/2. Also an attempt at reducing the temporal scale of the local wind forcing will be made. Both of these efforts should result in an increased eddy field which should be similar to the scale of the local wind forcing will be made. Both of these efforts should result in an increased eddy field which should be similar to the observations of the region. In addition a component of remote forcing will

be brought into the model. This forcing component will be induced by the results of the California Current region model. The anticipated results of this experiment are that the offshore propagation of features generated by the model will more closely approximate the observations as they did for the California Current model. The next logical step beyond this would be to assimilate the GEOSAT data directly into the model.

In conclusion, GEOSAT has proven to be one of the most successful oceanographic instruments of our time. The satellite provided data that will continue to provide useful information about the oceans for years to come. It has shown the importance of maintaining a satellite altimeter in orbit to provide near real time analysis of the sea surface in much the same way that meteorologic satellites do of the atmosphere. It also taught us many lessons on how to improve the next generation of radar altimeters to give us an even more accurate rendering of the ocean surface. We can only hope that the follow-on systems to GEOSAT will perform as well as it did in its 5-year life span.

References

- Aherns, D. C., *Meteorology Today: An Introduction to Weather, Climate and the Environment*, West, St. Paul, Minn., 1982.
- Barnett, T. P., Interaction of the monsoon and Pacific trade wind system at interannual time scales, I: The equatorial zone, *Mon. Weather Rev.*, *111*, 756-773, 1983.
- Calman, J., Introduction to sea surface topography from satellite altimetry, *Johns Hopkins APL Tech. Digest*, *8(2)*, 206-211, 1987.
- Cheney, R. E., Technical Memorandum, 1989.
- Cheney, R. E., B. C. Douglas, R. W. Agreen, L. Miller, D. L. Porter and N. S. Doyle, GEOSAT altimeter geophysical data record: User Handbook, *NOAA Tech. Memo. NOS NGS-46*, 1987.
- Cheney, R. E., L. Miller, R. W. Agreen, N. S. Doyle, B. C. Douglas, Monitoring tropical sea level in near real time with GEOSAT altimetry, *Johns Hopkins APL Tech. Digest*, *10(4)*, 362-367, 1989.
- Cummins, P. F. and L. A. Mysak, A quasi-geostrophic model of the northeast Pacific. Part I: A preliminary numerical experiment, *J. Phys. Oceanogr.* *18*, 1261-1286, 1988.
- Dodimead, A. J. and H. J. Hollister, Progress report of bottle releases in the northeast Pacific Ocean, *J. Fish. Res. Bd. Canada*, *15(5)*, 851-865, 1958.
- Doyle, N. S., R. E. Cheney, B. C. Douglas, R. W. Agreen, L. Miller and E. L. Timmerman, The NOAA GEOSAT geophysical data records: Summary of the third year of the exact repeat mission, *NOAA Tech. Memo. NOS NGS-51*, 1990.
- Emery, W. J., G. H. Born, D. G. Baldwin and C. L. Norris, Satellite-derived water vapor corrections for geosat altimetry, *J. Geophys. Res.*, *95(C3)*, 2953-2964, 1990.
- Emery, W. J. and K. Hamilton, Atmospheric forcing of interannual variability in the northeast Pacific ocean, connections with El Niño, *J. Geophys. Res.*, *95(C3)*, 2953-2964, 1990.
- Emery, W. J. and K. Hamilton, Atmospheric forcing of interannual variability in the northeast Pacific ocean, connections with El Niño, *J. Geophys. Res.*, *90(C1)*, 857-868, 1985.

- Gower, J. F. R., Sea-surface height anomalies in the north-east Pacific as observed with the Geosat altimeter: the Sitka eddy, In: *IGARRS '89, 12th Canadian Symposium on Remote Sensing, July 11, 1989, Vol. 2, IEEE Publ. No. 89CH2768-0, 1059-1062, 1989a.*
- Gower, J. F. R., Geosat altimeter observation of the distribution and movement of sea surface height anomalies in the north-east Pacific, In: *The global ocean, Abstracts from Oceans '89, Sept. 18-21, 1989, Seattle, Wash., Vol. 3, IEEE Publ. No. 89CH2780-5, 977-981, 1989b.*
- Hamilton, K. and L. A. Mysak, Possible Effects of the Sitka Addy on Sockeye (*Oncorhynchus nerka*) and Pink Salmon (*Oncorhynchus gorbuscha*) Migration off Southeast Alaska, *Can. J. Fish. Aquat. Sci.*, 43, 498-504, 1986.
- Heim, P. K. II, M. A. Johnson and J. J. O' Brien, The influence of the Alaskan gyre on the coastal circulation in the Gulf of Alaska, *J. Geophys. Res.*, in press 1991.
- Hickey, B. M., *Patterns and processes of circulation over the Washington continental shelf and slope, Coastal Oceanography of Washington and Oregon*, Elsevier, Amsterdam, 1989.
- Huyer, A., Seasonal variation in the temperature, salinity and density over the continental shelf off Oregon, *Limnol. and Oceanogr.*, 22(3), 442-453, 1977.
- Johnson, M. A. and J. J. O'Brien, Modelling the Pacific ocean, *The Int. J. Supercomputer Appl.*, 4(2), 37-47, 1990.
- Kelly, K. A., T. M. Joyce, D. M. Schubert and M. J. Caruso, The mean sea surface and geoid along the geosat subtrack from Bermuda to Cape Cod, *J. Geophys. Res.*, 96(C7), 12699-12709, 1991.
- Kirwan, A. D. Jr., G. J. McNally, E. Reyna and W. J. Merrell Jr., The near surface circulation of the eastern north Pacific. *J. Phys. Oceanogr.*, 8, 937-945, 1978.
- Miller, L., Personal communication on several occasions, 1990 and 1991.
- Mysak, L. A., El Niño, interannual variability and fisheries in the northeast Pacific, *Can. J. Fish. Aquat. Sci.*, 43, 464-497, 1986.
- Norton, J., D. McLain, R. Brainard and D. Husby, *The 1982-83 El Niño northeast Pacific, Can. J. Fish. Aquat. Sci.*, 43, 464-497, 1986.
- Norton, J., D. McLain, R. Brainard and D. Husby, *The 1982-83 El Niño event off Baja and Alta California and its ocean climate context, El Niño North: Niño Effects in the Eastern Subarctic Pacific Ocean*, Washington Sea Grant, Seattle, Wash., 44-72, 1985.

- O'Brien, J. J., A pilot monitoring system for El Niño, In: *EOS Transactions AGU*, Spring 1980.
- Pares-Sierra, A. and J. J. O'Brien, The seasonal and interannual variability of the California current system: A numerical model, *J. Geophys. Res.*, *94(C3)*, 3159-3180, 1989.
- Peffley, M. B. and J. J. O'Brien, A three-dimensional simulation of coastal upwelling off Oregon, *J. Phys. Oceanogr.*, *6*, 164-179, 1976.
- Pheobus, P. A. and J. D. Hawkins, The impact of the wet tropospheric correction and the interpretation of altimeter-derived ocean topography in the northeast Pacific, *J. Geophys. Res.*, *95(C3)*, 2939-2952, 1990.
- Royer, T. C., Baroclinic transport in the Gulf of Alaska, Part I: Seasonal variation of the Alaska current, *J. Mar. Res.*, *39*, 239-250, 1981.
- Shriver, J. F., M. A. Johnson, and J. J. O'Brien, Analysis of remotely forced oceanic Rossby waves off California, *J. Geophys. Res.* *96(C1)*, 749-757, 1991.
- Tabata, S., Evidence of a westward flowing countercurrent in the north Pacific ocean, *J. Fish. Res. Board Can.*, *33*, 2168-2196, 1976.
- Tabata, S., The anticyclonic baroclinic eddy off Sitka, Alaska in the northeast Pacific, *J. Phys. Oceanogr.* *12*, 1260-1282, 1982.
- Thomson, R. E., P. LeBlond, and W.J. Emery, Analysis of deep-drogued satellite tracked drifter measurements in the northeast Pacific, *Atmosphere-Ocean*, *28(4)*, 409-443, 1990.
- White, W. B., S. E. Pazen and M. Inoue, Hindcast/forecast of ENSO events based on the redistribution of observed and model heat content in western tropical Pacific, *J. Phys. Oceanogr.*, *17*, 264-280, 1987.
- White, W. B., C.-K. Tai and J. DiMento, Annual Rossby wave characteristics in the California current region from the GEOSAT exact repeat mission, *J. Phys. Oceanogr.*, *20*, 1297-1311, 1990.
- Zlotnicki, V., L.-L. Fu and W. Patzert, Seasonal variability in the global sea level observed with GEOSAT altimetry, *J. Geophys. Res.*, *94(C12)*, 17959-17969, 1989.
- Zlotnicki, V., L.-L. Fu and W. Patzert, Seasonal variability in the global sea level observed with GEOSAT altimetry, *J. Geophys. Res.*, *94(C12)*, 17959-17969, 1989.

Biographical Sketch

Paul Matthews was born in Concord, Ma. on July 7, 1962. In 1969 he moved to St. Petersburg, Fl., graduating from St. Petersburg Senior High School in June 1980. He attended The Bullis School in Potomac, Md. for one year of college preparatory courses on a Naval Academy Foundation scholarship. He graduated from the United States Naval Academy on May 22, 1985, receiving a B.S. degree in Oceanography. Upon graduation, he was commissioned an Ensign in the United States Navy, and entered flight training in Pensacola, Fl. and continued in Sacramento, Ca. In 1989 he was accepted to the Physical Oceanography program at the Florida State University in Tallahassee, Florida. He received his M.S. degree in Physical Oceanography in 1991. Upon completion of the requirements for the M.S. degree Paul will be returned to active duty with the United States Navy as an Oceanographer and will be stationed in Guam.